DOKUZ EYLUL UNIVERSITY
GRADUATE SCHOOL OF NATURAL AND APPLIED SCIENCES

SYNTHESIS, CHARACTERIZATION AND ELECTRICAL PROPERTIES OF PIEZOELECTRIC MATERIALS BY SOL-GEL TECHNIQUE

by
Tülin GÖNÜLŞEN

February, 2006
İZMİR

SYNTHESIS, CHARACTERIZATION AND ELECTRICAL PROPERTIES OF PIEZOELECTRIC MATERIALS BY SOL-GEL TECHNIQUE

A Thesis Submitted to the
Graduate School of Natural and Applied Sciences of Dokuz Eylül University
In Partial Fulfillment of the Requirements for the Degree of Master of Science
in Metallurgical and Materials Engineering, Materials Science Program

by
Tülin GÖNÜLŞEN

February, 2006
İZMİR

M.Sc THESIS EXAMINATION RESULT FORM

We have read the thesis entitled **"SYNTHESIS, CHARACTERIZATION AND ELECTRICAL PROPERTIES OF PIEZOELECTRIC MATERIALS BY SOL-GEL TECHNIQUE"** completed by **Tülin GÖNÜLŞEN** under supervision of **Prof. Dr. Ahmet ÇAKIR** and we certify that in our opinion it is fully adequate, in scope and in quality, as a thesis for the degree of Master of Science.

Prof. Dr. Ahmet ÇAKIR

Supervisor

Yrd. Doç. Dr. Müntar Gölen

(Jury Member)

Doç. Dr. Erdal Çelik

(Jury Member)

Prof.Dr. Cahit HELVACI

Director

Graduate School of Natural and Applied Science

ACKNOWLEDGEMENTS

First of all, I would like to thank to Prof. Dr. Ahmet ÇAKIR, my supervisor, for helps and comments from the first day of my project until the last day.

Secondly, I am grateful to Assoc. Prof. Dr. Erdal Çelik who helped me during experimental studies and all members of Department of Metallurgical and Materials Engineering for their friendship supports.

Finally, I would like to express my deepened gratitude for whole support and understanding that I received from my parents during the past years.

Tülin GÖNÜLŞEN

SYNTHESIS, CHARACTERIZATION AND ELECTRICAL PROPERTIES OF PIEZOELECTRIC MATERIALS BY SOL-GEL TECHNIQUE

ABSTRACT

Piezoelectric materials are attractive for microelectromechanical systems (MEMS) applications, inasmuch as they have good properties capable for actuation or sensing in these applications. Moreover, thin film micro actuator or sensor of these materials is interesting because of simple design and compatible to mass production processes. With this regard, lead titanate thin films were successfully fabricated on glass and stainless steel substrates using sol–gel coating method. A sol was prepared by mixing lead acetate trihydrate, titanium 4-isopropoxide and glacial acetic acid in ethylene glycol. The films were obtained by dipping and dropping techniques. The obtained gel films were dried at 300 degree of a Celsius for 10 minutes. The coating and drying processes were repeated many times to get desired film thickness and the oxide thin films were finally annealed at 600 degree of a Celsius for 60 minutes in air. The obtained films were characterized by TG-DTA, XRD, SEM/EDS and spectrophotometer. In addition, dielectric properties of the films were investigated by using impedance.

It was found that homogeneous and perovskite lead titanate thin films were prepared by a sol-gel technique under simple production conditions. Perovskite phase started to develop at temperature ranging between 400 and 500 degree of a Celsius and the pure perovskite lead titanate phase was fully developed at 600 degree of a Celsius for 1 hour in air. The optimum surface morphology of the film without any cracks or defects could be obtained in solution with maximum amount of solvent. It was determined that the value of dielectric constant and dielectric loss depended on film thickness.

Keywords: Thin film, lead titanate, sol–gel, perovskite, microstructure, dielectric.

SOL-GEL TEKNİĞİ İLE ÜRETİLEN PİEZOELEKTRİK MALZEMELERİN SENTEZLENMESİ, KARAKTERİZASYONU VE ELEKTRİSEL ÖZELLİKLERİ

ÖZ

Piezoelektrik malzemeler sahip oldukları güzel algılama ve hareketlenme kabiliyetleri kadar mikro elektro mekaniksel sistemlerin uygulamaları için de çok ilgi çekicidir. Ayrıca, bu malzemelerin harekete geçirici ve algılayıcı ince filmleri, basit tasarım ve parça üretim yöntemine olan uyumundan dolayı enteresandır. Bu bakış ile, kurşun titanyum oksit ince filmleri, cam ve paslanmaz çelik altlıklar üzerine sol-jel kaplama yöntemiyle başarıyla imal edilmiştir. Solüsyon, kimyasal bileşiminde üç mol su bulunduran kurşun asetat, titanyum dört-isopropoxide ve glasiel asetik asidin etilen glikol içerisinde karışımıyla hazırlanmıştır. Filmler daldırma ve damlatma teknikleriyle oluşturulmuştur. Elde edilen bu jel filmler 300 derecede 10 dakika kurutulmuştur. Kaplama ve kurutma işlemleri istenilen kalınlığı elde etmek için birçok kez tekrarlanmış ve son olarak, oksit ince filmler hava ortamında 600 derecede 60 dakika tavlanmıştır. Farklı film kalınlıklarının ve çözücü yoğunluklarının ince filmlerde yüzey morfolojisine olan etkileri incelenmiştir. Elde edilen filmler TG/DTA, XRD, SEM/EDS ve spektrometre ile karakterize edilmiştir. İlaveten, filmlerin elektriksel özellikleri empedans kullanılarak araştırılmıştır.

Tabii üretim şartları altında homojen ve perovskit yapılı kuşun titanyum oksit filmlerinin hazırlandığı bulunmuştur. Dielektrik sabiti ve dielektrik kaybı film kalınlığına bağlı olarak saptanmıştır. Perovskit fazı 400-500 derece arasındaki sıcaklık bölgesinde gelişmeye başlamış ve tamamen saf perovskit kurşun titanyum oksit fazı hava ortamında 600 derecede 1 saatte geliştirilmiştir. Çatlak ve hatalar içermeyen optimum yüzey morfolojisine sahip film, çözeltisinde en yüksek miktarda çözücü içeren için bulunabilmiştir. Dielektrik sabiti ve dielektrik kaybı değerlerinin film kalınlığına bağlı olduğu saptanmıştır.

Anahtar sözcükler: İnce film, kurşun titanyum oksit, sol-gel, perovskite, mikroyapı.

CONTENTS

page

CHAPTER ONE
INTRODUCTION

Piezoelectric materials, often referred to as “smart materials” are materials that undergo transformations through physical interactions. An alternate definition is that a smart material is a material that senses a change in its environment and through the use of a feedback system, adapts to correct or eliminate such a change. Piezoelectricity stems from the Greek word “piezo” for pressure. It follows that a piezoelectric material develops a potential across its boundaries when subjected to a mechanical stress (or pressure), and vice versa, when an electric field is applied to the material, a mechanical deformation ensues. Piezoelectric materials therefore fall in the class of smart materials. Ferroelectricity is a subgroup of piezoelectricity, where a spontaneous polarization exists that can be reoriented by application of an AC electric field (Jordan et al., 2001).

Piezoelectric materials are attractive for microelectromechanical systems (MEMS) applications, inasmuch as they have good properties capable for actuation or sensing in these applications. Moreover, thin film micro actuator or sensor of these materials is interesting because of simple design and compatible to mass production processes (He et al., 2003).

The piezoelectric effect was discovered by Pierre and Jacques Curie and first reported in 1880. The Curies studied naturally occurring crystals such as quartz, Rochelle salt and tourmaline. They later observed the converse effect, which was predicted from thermodynamic principles by Lipmann in 1881. The direct effect may be used in sensing applications, while the indirect effect may be used in actuation and acoustic transduction. The piezoelectric effect is caused by an asymmetry in the unit cell and the resulting relationship between mechanical distortion and electric dipole separation (Prasad et al., 2005)

Quartz is a well-known single crystal material depicting such piezoelectric effects. However, strong piezoelectric effects can be induced in polycrystalline lead zirconate

titanate based ferroelectric ceramic materials. These materials are represented by the formula ABO_3 perovskite crystalline structure where in A-site denotes large divalent metal ion such as Pb and B-site denotes smaller tetravalent ion such as Ti or Zr. This class of ceramic materials possesses several advantages over single crystals including higher piezoelectric coefficients, ease of fabrication into components of any shape and size, mechanically hard and robust, chemically inert and completely unaffected by atmospheric humidity. In contrast, single crystals must be cut along certain crystallographic direction, thus limiting their possible geometrical shapes (Jordan et al., 2001).

Lead titanate ($PbTiO_3$) is a perovskite ferroelectric with piezoelectric properties. People paid great attention on it because it possesses a high Curie temperature (490 °C), relatively high piezoelectric properties. Ferroelectric thin films can be fabricated by using various techniques such as sputtering, chemical vapor deposition (CVD) and metal-organic deposition (MOD). These methods involve drawbacks such as expensive equipment, complicated chemistry, and high reaction temperatures. Other problems with these techniques are difficulties in adjusting composition for the optimization of properties, inhomogeneities, and the fabrication of suitable targets. The major disadvantage of these methods is the difficulty in controlling the stoichiometry while fabricating multicomponent oxide films. This problem results from differences in the sputtering rates of the components or the vapor pressures of the CVD precursor reagents (Wu et al., 1998).

Sol-gel processing has recently been receiving attention as an alternative method for the fabrication of ferroelectric thin films. This technique provides a solution to some of the problems encountered in conventional fabrication techniques. Modern ceramic technology requires high purity which can be obtained by the sol-gel process. Extremely homogeneous thin films with lower processing temperatures can be synthesized because the precursors are mixed as liquids. Also, compositions can be easily adjusted for the optimization of properties of the films. Another advantage of sol-gel is that it facilitates the fabrication of films on substrates with large or complex areas (Bao et al., 2002).

In the present work, we investigated synthesis, characterization and electrical properties of $PbTiO_3$ thin films on glass and stainless steel substrates using different solutions of lead acetate trihydrate, titanium (IV) isopropoxide, glacial acetic acid and ethylene glycol via sol–gel process. The phase structure, thermal, microstructure and surface properties of the coatings were characterized using X-ray diffractometer (XRD), differential thermal analysis/thermogravimetric (DTA/TG), scanning electron microscopy (SEM) with attached energy dispersive spectroscopy (EDS) and spectrophotometer. Their electrical properties were investigated by impedance. As a result, $PbTiO_3$ thin films were successfully fabricated on glass and stainless steel substrates using sol-gel technique.

CHAPTER TWO
PIEZOELECTRIC CERAMICS

2.1 Piezoelectricity

Piezoelectricity is a linear effect that is related to the microscopic structure of the solids. The microscopic origin of the piezoelectric effect is the displacement of ionic charges within a crystal structure resulting in electric dipole behaviors (polarization).

In single crystals of some ceramic materials become electrically polarized when they are strained. In the absence of external strain, the charge distribution within the crystal is symmetric and the net electric dipole moment is zero. However when an external stress is applied, the charges are displaced creating an unsymmetrical distribution. One side of the crystal derives a net positive charge and the opposite side derives a net negative charge. A net polarization develops and results in an internal electric field. This effect is referred to as piezoelectricity. Conversely, an applied electric field can cause a piezoelectric material to change dimensions (as a strain) directly proportional to an applied field. This phenomenon is known as electrostriction or the reverse piezoelectric effect to a first approximation. The polarization is proportional to the stress and the effect is said to be 'direct'. A material can only be piezoelectric if the unit cell has no center of symmetry (anisotropic structure) (Jordan, & Ounaies, 2001).

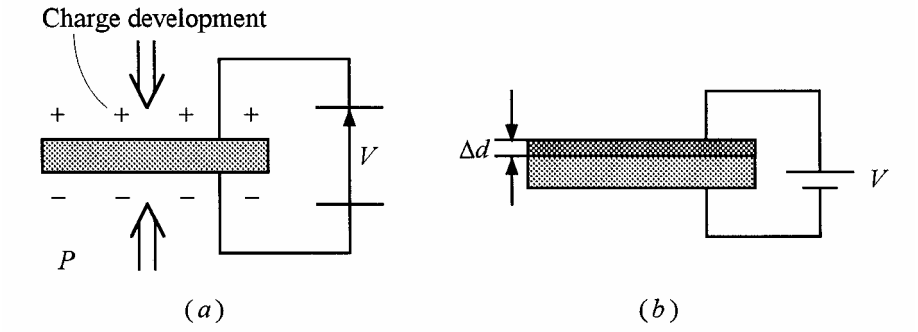

Figure 2.1 (a) The direct and (b) the inverse piezoelectric effect (Barsoum, 1997).

The 32 crystal groups can be further classified into (a) crystals having a center of symmetry and (b) crystals which do not possess a center of symmetry. Crystals with a center of symmetry classified in the 11 point groups labeled as centrosymmetric. These point groups do not show polarity. For these an applied stress results in symmetrical ionic displacements so that there is no net change in dipole moment. The remaining 21 point groups do not have a center of symmetry (i.e. non-centrosymmetric) and 20 of these are piezoelectric. One class, although lacking of a center of symmetry, is not piezoelectric because of other combiner symmetry elements. A crystal having no center of symmetry possesses one or more crystallographically unique directional axes (Richerson, 1992).

2.2 Pyroelectricity

Pyroelectric crystals are a special class of piezoelectric crystals. They contain within their crystal structure a preexisting spontaneous polarization along one crystallographic direction. The value of this spontaneous polarization depends on the temperature. Heating of the crystals results in mechanical deformation due to thermal expansion, which results in a change in the extent of polarization. This is called the pyroelectric effect which was first discovered in tourmaline by Brewster in 1824. The prefix “pyro” is Greek for “fire”, so pyroelectric translates to “fire electricity”, that is, electricity released by heat (Safari, Panda, & Janas, n.d.).

Of the 20 piezoelectric crystal classes, 10 are pyroelectric. Although a crystal with polar axes (20 non centrosymmetric point groups) shows the piezoelectric effect, it is not enough for it to have a spontaneous polarization vector. It could be due to the canceling of the electric moments along the different polar axes to give a zero net polarization. Only crystals with a unique polar axis show a spontaneous polarization vector P_s along this axis. Examples of pyroelectric crystals include wurtzite (hexagonal ZnS), tourmaline, Rochelle salt, triglycine sulfate, $BaTiO_3$, $Pb(Zr,Ti)O_3$, and lithium sulfate (Richerson, 1992).

The pyroelectric effect can be described in terms of the pyroelectric coefficient π. A small change in the temperature ΔT, in a crystal, in a gradual manner, leads to a change in the spontaneous polarization vector ΔP_s given by,

$$\Delta P_s = \pi.\Delta T \qquad (2.1)$$

Figure 2.2 shows the variation of the spontaneous polarization P_s with temperature for a $BaTiO_3$ ferroelectric crystal. An increase in the temperature leads to a decrease in the spontaneous polarization $BaTiO_3$ has a negative pyroelectric coefficient. The polarization suddenly falls to zero on heating the crystal above the Curie point (Safari et al., n.d.).

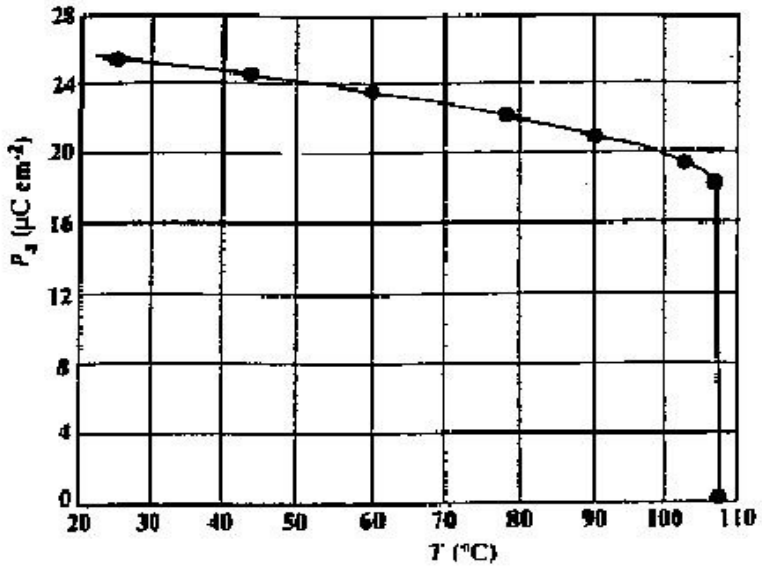

Figure 2.2 The temperature dependence of spontaneous polarization P_s for $BaTiO_3$ ferroelectric crystal (Safari et al., n.d.).

An important pyroelectric material is $LiTaO_3$. Most pyroelectric materials lose their pyroelectric behavior as the temperature is increased to a few hundred degrees C. $LiTaO_3$ retains its pyroelectric behavior to 609 ^oC (1128 ^oF). It can therefore be used over a broad temperature range for extremely accurate measurement of temperature changes. Changes on the order of 10^{-6} ^oC can be detected. As a result, $LiTaO_3$ has been developed into a scanning microcalorimeter capable of sensitivity in the submicrocalorie range. It has also been used as a high-sensitivity micro

enthalpymeter for monitoring catalytic process. Both devices involve a 50 μm (0.002 in.) thick chip of $LiTaO_3$ mounted on a ceramic substrate and coated with a thin-film NiCr heater element. The size of the overall device is about 5 mm x 5 mm x 0.5 mm (Richerson, 1992).

Other applications for pyroelectric ceramics include optical sensors, thermal bolometers for infrared measurement, and devices for gas-flow measurement.

2.3 Ferroelectricity

Ferroelectric materials are a subclass of pyroelectric crystals, thus, some piezoelectric materials are also ferroelectric. A huge jump in the research on ferroelectric materials came in the 1950's, leading to the widespread use of barium titanate ($BaTiO_3$) based ceramics in capacitor applications and piezoelectric transducer devices. Since then, many other ferroelectric ceramics including lead titanate ($PbTiO_3$), lead zirconate titanate (PZT), lead lanthanum zirconate titanate (PLZT), and relaxor ferroelectrics like lead magnesium niobate (PMN) have been developed and utilized for a variety of applications. With the development of ceramic processing and thin film technology, many new applications have emerged. The biggest use of ferroelectric ceramics have been in the areas such as dielectric ceramics for capacitor applications, ferroelectric thin films for non volatile memories, piezoelectric materials for medical ultrasound imaging and actuators, and electro-optic materials for data storage and displays (Safari et al., n.d.).

2.3.1 General Properties of Ferroelectrics

Like the pyroelectric crystals, the ferroelectric crystals contain a spontaneous polarization developed by the value of the net dipole moment per unit volume for the dipoles pointing in a given direction or by the value of the charge per unit area on the surface perpendicular to the axis of spontaneous polarization.

2.3.1.1 Ferroelectric Domains and Hysteresis Loop

Ferroelectric crystals retain a dipole even after an applied voltage has been removed. If the magnitude and direction of P_s can be reversed by an external electric field, then such crystals are said to show ferroelectric behavior. Hence, all single crystals and successfully poled ceramics which show ferroelectric behavior are pyroelectric, but not vice versa. For example tourmaline shows pyroelectricity but is not ferroelectric (Safari et al., n.d.).

Ferroelectric crystals possess regions with uniform polarization called ferroelectric domains. Within a domain, all the electric dipoles are aligned in the same direction. There may be many domains in a crystal separated by interfaces called domain walls. A ferroelectric single crystal, when grown, has multiple ferroelectric domains. A single domain can be obtained by domain wall motion made possible by the application of an appropriate electric field. A very strong field could lead to the reversal of the polarization in the domain, known as domain switching (Safari et al., n.d.).

The main difference between pyroelectric and ferroelectric materials is that the direction of the spontaneous polarization in ferroelectrics can be switched by an applied electric field (Jordan, & Ounaies, 2001).

Applying a large alternating electric field causes the polarization to reverse, and this gives rise to the ferroelectric hysteresis loop, relating P is the polarization in units such as $\mu C/cm^2$ to E is the applied electric field in units such as kV/cm. A typical field-polarization loop is illustrated in Figure 2.3. As the electric field strength is increased, the domains start to align in the positive direction giving rise to a rapid increase in the polarization (OB). At very high field levels, the polarization reaches a saturation value (P_{sat}). The polarization does not fall to zero when the external field is removed. At zero external field, some of the domains remain aligned in the positive direction, hence the crystal will show a remnant polarization P_r. The crystal cannot be completely depolarized until a field of magnitude OF is applied in

the negative direction. The external field needed to reduce the polarization to zero is called the coercive field strength E_c. If the field is increased to a more negative value, the direction of polarization flips and hence a hysteresis loop is obtained. The value of the spontaneous polarization P_s (OE) is obtained by extrapolating the curve onto the polarization axes (CE) (Safari et al., n.d.).

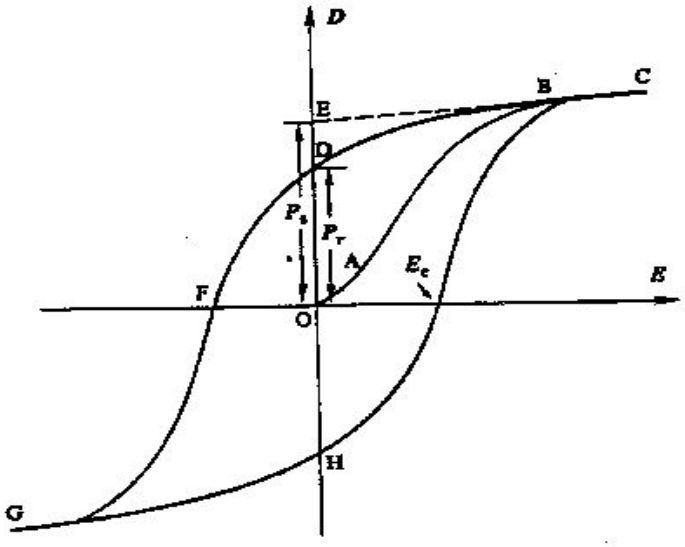

Figure 2.3 A Polarization vs. Electric Field (P-E) hysteresis loop for a typical ferroelectric crystal. (Safari et al., n.d.).

Generally, the existence of the P-E loop is considered as evidence towards establishing that a material is ferroelectric. A Sawyer-Tower circuit or its modified version is commonly used to obtain a P-E loop. An AC voltage is applied to the electroded sample; the resulting charge stored on the sample is determined by means of a large reference capacitor placed in series with the sample. An electrometer can be used to detect the voltage across the capacitor; by multiplying this voltage with the value of the reference capacitor, the charge across the sample results. The reference capacitor should be 100 to 1000 times the value of the capacitance of the sample. It is noted that ferroelectric hysteresis loops are both frequency and temperature dependent (Jordan, et al. 2001).

In addition to the P-E loop, polarization switching leads to strain-electric field hysteresis. A typical strain-field response curve is shown in Figure 2.4. The shape resembles that of a butterfly, and it is often referred to as the "butterfly loop". As the electric field is applied, the converse piezoelectric effect dictates that a strain results. As the field is increased, the strain is no longer linear with the field as domain walls start switching (Jordan et al., 2001).

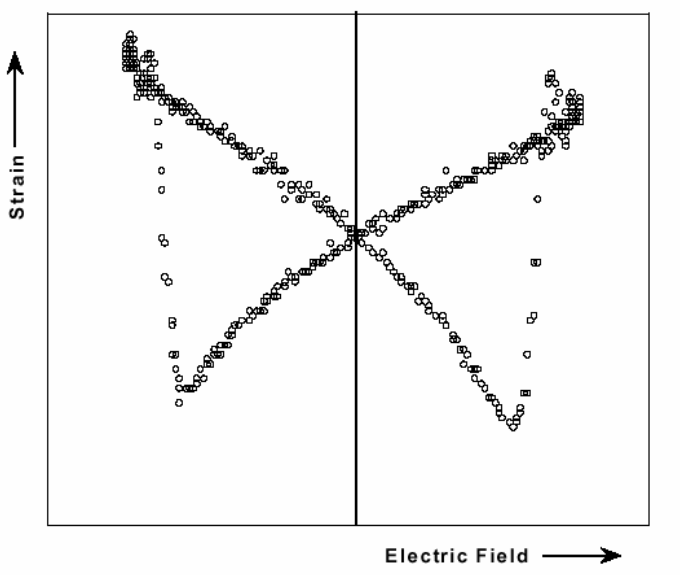

Figure 2.4 Butterfly loop indicating switching (Jordan et al., 2001).

2.3.1.2 Curie Point and Phase Transitions

All ferroelectric materials have a transition temperature called the Curie point (T_c). At a temperature $T > T_c$ the crystal does not exhibit ferroelectricity (paraelectric), while for $T < T_c$ it is ferroelectric (polar). On decreasing the temperature through the Curie point, a ferroelectric crystal undergoes a phase transition from a non-ferroelectric phase to a ferroelectric phase. If there are more than one ferroelectric phases, the temperature at which the crystal transforms from one ferroelectric phase to another is called the transition temperature. Near the Curie point or transition temperatures, thermodynamic properties including dielectric, elastic, optical, and thermal constants show an irregular behavior. This is due to a distortion in the crystal as the phase structure changes. The temperature dependence

of the dielectric constant above the Curie point ($T > T_c$) in ferroelectric crystals is governed by the Curie-Weiss law:

$$\varepsilon = \varepsilon_0 + C/(T - T_0) \qquad (2.2)$$

Where ε is the permittivity of the material, ε_0 is the permittivity of vacuum; C is the Curie constant and T_o is the Curie temperature. The Curie temperature T_o is different from the Curie point T_c. T_o is a formula constant obtained by extrapolation, while T_c is the actual temperature where the crystal structure changes (Safari et al., n.d.).

The dielectric permittivity often has a peak at T_c and linearly decreases according to the Curie-Weiss law. The very large permittivity values that are characteristics of ferroelectric materials are greatly exploited in many applications, most widely in the multilayer-capacitor industry (Richersan, 1992).

All crystals that are ferroelectric are pyroelectric and piezoelectric; all crystals that are pyroelectric are piezoelectric; but not all piezoelectric crystals are pyroelectric or ferroelectric. Ferrolectric behaviour is dependent on the crystal structure. The crystal must be noncentric and must contain alternate atom positions or molecular orientations to permit the reversal of the dipole and the retention of polarization after the voltage is removed. To appreciate the difference between a piezoelectric and a ferroelectric crystal it is instructive to compare Figure 2.5.c and e. An unstressed piezoelectric (Figure 2.5.c) crystal only develops a dipole when stressed (Figure 2.5.d) as a consequence of its symmetry. A ferroelectric crystal, on the other hand, possesses a dipole even in the unstressed state (Figure 2.5.e). The application of a stress only changes the value of the polarization (Figure 2.5.f) (Barsoum, 1997).

The ceramic may be made piezoelectric in any chosen direction by a poling treatment which involves exposing it to a strong electric field at a temperature slightly below the Curie point (Figure 2.7.b). Under the action of this field, domains most nearly aligned with the field will grow at the expense of other domains. The

material will also lengthen along the poling axis and contract in both directions perpendicular to it (Figure 2.6) (Jorden et al., 2001).

When the field is removed (Figure 2.7.c), the dipoles remain locked in approximate alignment, giving the ceramic material a remnant polarization and a permanent deformation (i.e. making it anisotropic). The poling treatment is usually the final treatment of PZT component manufacture.

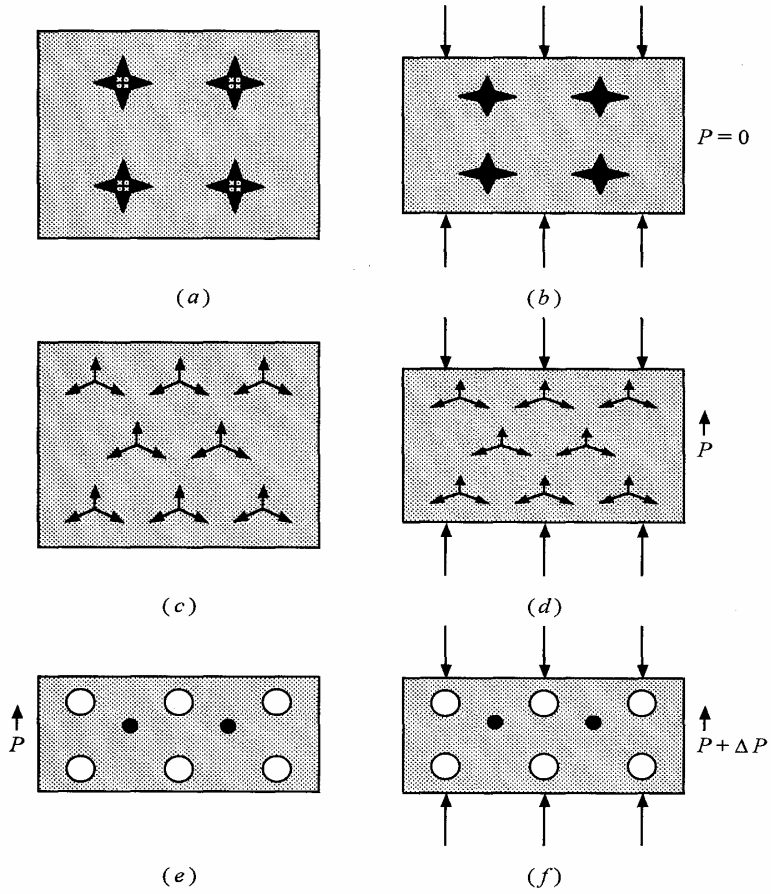

Figure 2.5 (a) Unstressed centrosymmetric crystal.The arrows represent dipole moments. (b) Applying a stress to such a crystal cannot result in a polarization. (c) Unstressed noncentrocymmetric crystal, i.e., piezoelectric. Note that this structure is not ferroelectric because it does possess a permanent dipole. (d) Stressed crystal develops a polarization as shown. (e) Unstressed polar crystal, i.e., ferroelectric, possesses a permanent dipole even in the unstressed state. (f) Stressed ferroelectric crystal. The applied stress changes the polarization by ΔP (Barsoum, 1997).

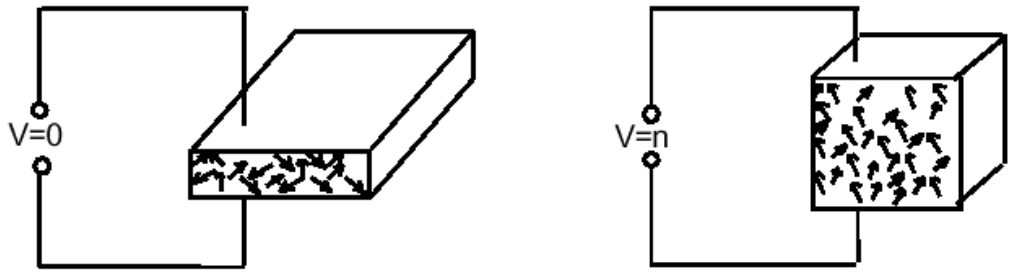

Figure 2.6 Poling of a piezoelectric and ferroelectric ceramic (Jorden et al., 2001).

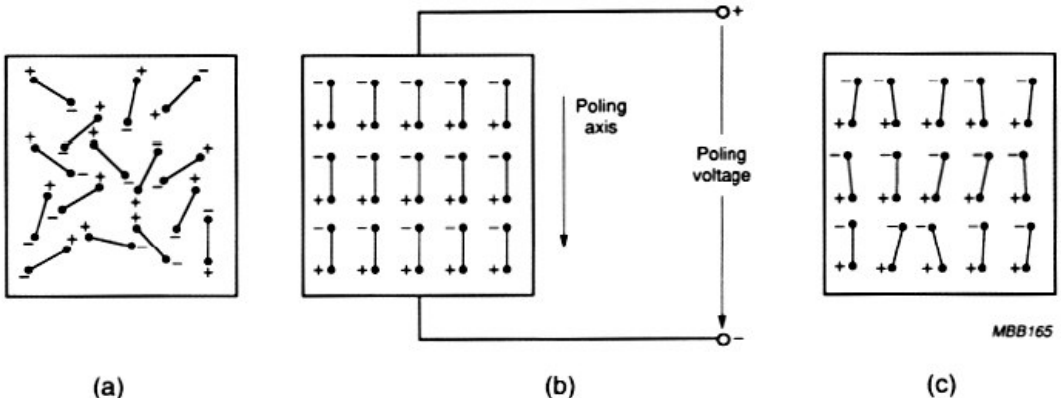

Figure 2.7 Electric dipole moments in Weiss domains; (a) before polarization, (b) during polarization, (c) after polarization (Piezoelectric ceramics properties & applications, n.d.).

The material can be depoled by reversing the poling voltage, increasing the temperature beyond the materials Currie point, or by inducing a large mechanical stress.

2.4 Basic Behaviour of a Piezoelectric Ceramic Body

Figure 2.8 illustrates the behaviour of a PZT cylinder polarized along its axis. For clarity, the magnitude of the effect has been exaggerated. Figure 2.8(a) shows the cylinder under no-load conditions. If an external force produces compressive or tensile strain in the material, the resulting change in dipole moment causes a voltage to appear between the electrodes. If the cylinder is compressed so that it resumes its original form, i.e. before poling, the voltage will have the same polarity as the poling

voltage (Figure 2.8(b)). If it is stretched, the voltage across the electrodes will have opposite polarity to the poling voltage (Figure 2.8(c)). These are examples of generator action: the conversion of mechanical energy into electrical energy. Examples of piezoelectric induced generator action can be found in cigarette and gas lighters, gramophone pick-ups, accelerometers, hydrophones and microphones. If a voltage of opposite polarity to the poling voltage in applied to the electrodes, the cylinder will shorten (Figure 2.8(d)). If the applied voltage has the same polarity as the poling voltage, the cylinder will lengthen (Figure 2.8(e)). Finally, if an alternating voltage is applied to the electrodes, the cylinder will grow and shrink at the same frequency as that of the applied voltage (Figure 2.5(f)). These are examples of motor action: conversion of electrical energy into mechanical energy (Piezoelectric ceramics properties & applications, n.d.).

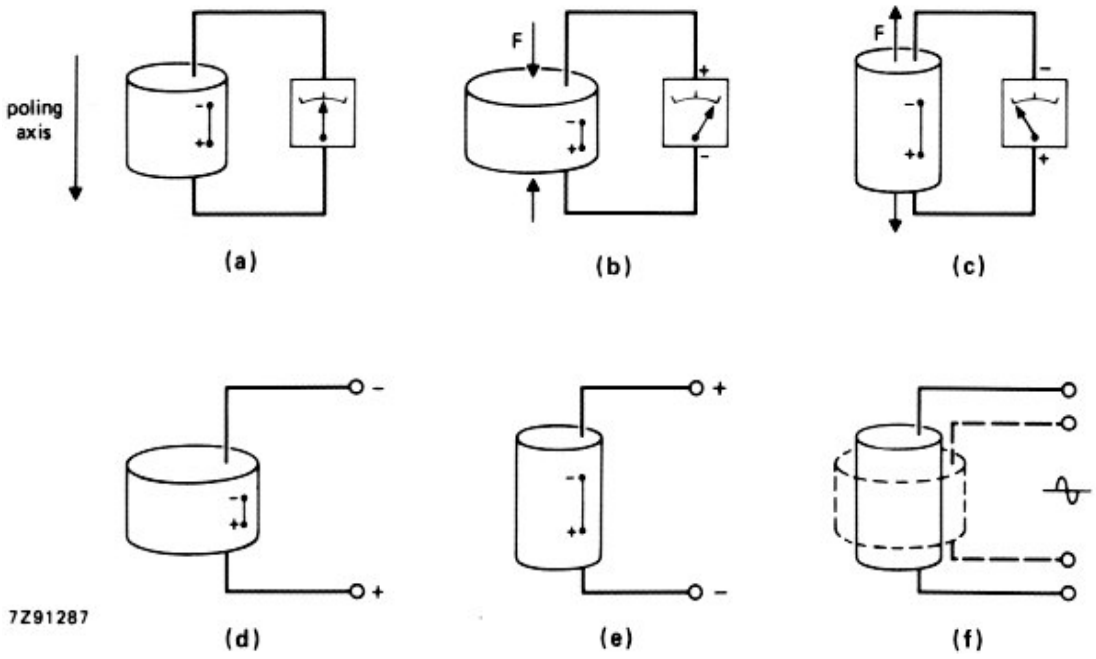

Figure 2.8 The piezoelectric effect in a cylindrical body of piezoelectric ceramic (Piezoelectric ceramics properties & applications, n.d.).

The basic equations that describe these two effects in regard to electric and elastic properties;

$$D = dT + \varepsilon^{T}E \quad \text{(generator)} \qquad (2.3)$$

$$S = s^{E}T + dE \quad \text{(motor)} \qquad (2.4)$$

Where D is the electric displacement, T is the stress, E is the electric field, S is the strain, s is the elastic compliance (inverse of modulus of elasticity), ε is the dielectric constant (permittivity) and the superscripts denote the parameter held constant (Moulson et al., 1990).

2.5 Piezoelectric Properties

Since piezoelectric ceramics are anisotropic, their physical constants (elasticity, permittivity etc.) are tensor quantities and relate to both the direction of the applied stress, electric field etc., and to the directions perpendicular to these. For this reason the constants are generally given two subscript indices which refer to the direction of the two related quantities (e.g.stress and strain for elasticity, electric displacement and field for permittivity). The first subscript gives the direction of the electrical field associated with the voltage applied, or the charge or the voltage produced. The second subscript gives the direction of the mechanical stress or the strain (Piezoelectric ceramics properties & applications, n.d.).

To identify directions in a piezoelectric element, three axes termed as 1, 2 and 3; which are analogous to the classical three dimensional orthogonal set of axes X, Y and Z are used. Material properties along the 1 and 2 axes are identical to each other but different from those along the 3 axis. For maintaining simplicity, references are made only to the 3 and 1 directions. The poling or 3 - axis is invariably taken parallel to the direction of polarisation within the ceramic (Figure 2.9(a)). The polar axis is induced during the manufacturing process by treatment with a high voltage DC field applied between the pair of electroded faces to align the domains of the material in the direction of the field (Sparkler piezoceramics, n.d.).

The polarisation vector P is represented by an arrow pointing from the positive to the negative poling electrode. In shear mode operations, the poling electrodes are

later removed and replaced by a set of electrodes on the second pair of the faces. The 3-axis is not altered, but it becomes parallel to the new electrode faces as seen on the finished element (Figure 2.9(b)) (Sparkler piezoceramics, n.d.).

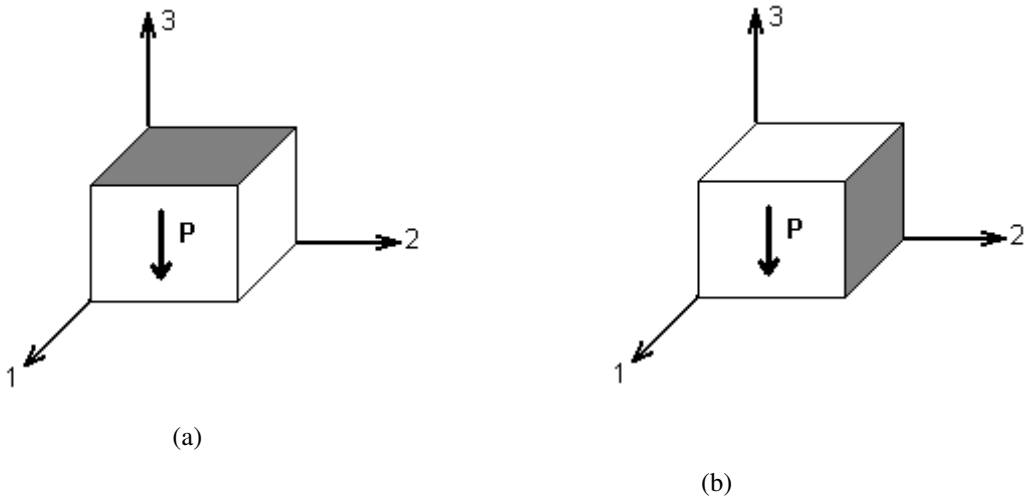

(a) (b)

Figure 2.9 Designation of the axis and directions of the electrodes (Sparkler piezoceramics, n.d.).

The equations, which define this relationship, are the piezoelectric equations.

$$D_i = d_{ij} T_j \qquad \text{(direct effect)} \qquad (2.5)$$

$$S_j = d_{ij} E_i \qquad \text{(converse effect)} \qquad (2.6)$$

Where D_i is the electric displacement (polarization) generated along the i-axis in response to the applied stress T_j, and d_{ij} is the piezoelectric coefficient. For the converse effect, S_j is the strain generated in a particular orientation of the crystal on the application of electric field E_i along the i-axis (Safari et al., n.d.).

2.5.1 Parameters for Piezoelectric Ceramics

When considering the electromechanical effects, the interesting parameters of piezoelectric materials are the piezoelectric charge coefficients, the piezoelecric

voltage coefficients and the piezoelectric coupling factors (Piezoelectric ceramics properties & applications, n.d.).

2.5.1.1 Piezoelectric Charge Coefficient (d constant)

The piezoelectric charge constant is defined as the electric charge collected on the electrodes per applied unit mechanical stress that induced the charge (Prasad et al., 2005).

$$d_{ij} = \frac{\text{short circuit charge density}}{\text{applied mechanical stress}} = \frac{\text{coulombs/meter}^2}{\text{newtons/meter}^2} = \frac{\text{coulombs}}{\text{newton}} \qquad (2.7)$$

In the converse effect, it is the mechanical strain experienced by the material per unit electric field applied to it (Prasad et al., 2005).

$$d_{ij} = \frac{\text{strain developed}}{\text{applied electric field}} = \frac{\text{meter/meter}}{\text{volt/meter}} = \frac{\text{meter}}{\text{volt}} \qquad (2.8)$$

The first subscript refers to the direction of polarization generated in the material (at E = 0) or to the applied field strength, the second refers respectively to the direction of the applied stress or to the direction of the induced strain.

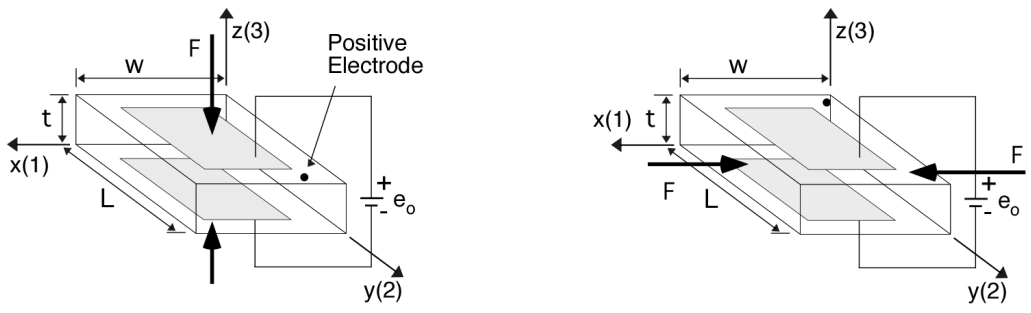

(a) d_{33} (b) d_{31}

Figure 2.10 Piezoelectric coordinate system for (a) d_{33} and, (b) d_{31} constants.

d_{33} is the induced polarization per unit applied stress in direction 3. Alternatively it is the induced strain per unit electric field in direction 3. d_{31} is the induced polarization in direction 3 per unit stress applied in direction 1. Alternatively it is mechanical strain induced in the material in direction 1 per unit electric field in direction 3.

High d-constants are desirable in materials utilized as actuators, as used in motional and vibrational applications.

2.5.1.2 Piezoelectric Voltage Coefficient (g constant)

The piezoelectric voltage constant is defined as the electric field generated in a material per unit mechanical stress applied to it (Sparkler piezoceramics, n.d.).

$$g_{ij} = \frac{\text{open circuit electric field}}{\text{applied mechanical stress}} = \frac{\text{volt/meter}}{\text{newton/meter}^2} = \frac{\text{volt} - \text{meter}}{\text{newton}} \qquad (2.9)$$

Alternatively, it is the mechanical strain experienced by the material per unit electric displacement applied to it.

$$g_{ij} = \frac{\text{strain developed}}{\text{applied charge density}} = \frac{\text{meter/meter}}{\text{coulombs/meter}^2} = \frac{\text{meter}^2}{\text{coulomb}} \qquad (2.10)$$

Output voltage is applied by multiplying the calculated electric field by the thickness of the ceramic between the electrodes. The first subscript indicates the direction of the generated voltage and the second indicates the direction of the force.

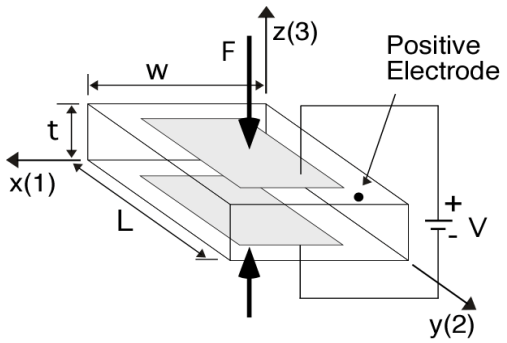

Figure 2.11 Piezoelectric coordinate system for g_{33} constant.

For example: g_{33} is the induced electric field in direction 3 (parallel to the direction in which ceramic element is polarized) per unit stress applied in direction 3.

Alternatively it is the induced strain in direction 3 per unit electric displacement applied in direction 3. g_{31} is the induced electric field in direction 3 (parallel to the direction in which ceramic element is polarized) per unit in direction 1. Alternatively it is the induced strain in direction 1 per unit electric displacement applied in direction 3.

Because the strength of the induced electric field produced by a piezoelectric material in response to an applied physical stress is the product of the value for the applied stress and the value for g, g is important for assessing a material's suitability for sensing (sensor) applications (Prasad et al., 2005).

The g constant is related to the d constant via the relationship,

$$g = \frac{d}{K.\varepsilon_0} \quad (2.11)$$

where K is the relative dielectric constant and ε_0 permittivity of free space.

2.5.1.3 Dielectric Constant and Dielectric Loss

The permittivity, or dielectric constant, ε, for a piezoelectric ceramic material is the dielectric displacement per unit electric field (Dielectric, n.d.).

$$\varepsilon = \frac{D}{E} = \frac{\text{coulombs/ meter}^2}{\text{volts/ meter}} = \frac{\text{farads}}{\text{meter}} \quad (2.12)$$

ε^T is the permittivity at constant stress, ε^S is the permittivity at constant strain. The first subscript to ε indicates the direction of the dielectric displacement; the second

the direction of the electric field (Piezoelectric ceramics properties & applications, n.d.).

The relative dielectric constant, K, is the ratio of ε, the amount of charge that an element constructed from the ceramic material can store, relative to the absolute dielectric constant, ε_0 , the charge that can be stored by the same electrodes when separated by a vacuum, at equal voltage ($\varepsilon_0 = 8.85*10^{-12}$ farad / meter) (Dielectric, n.d.).

$$K' = \frac{\text{permittivity of material}}{\text{permittivity of free space}} = \frac{\varepsilon}{\varepsilon_0} = \varepsilon_r \qquad (2.13)$$

ε_{11}^{T} is the permittivity for dielectric displacement and electric field in direction 1 (perpendicular to direction in which ceramic element is polarized), under constant stres. ε_{33}^{S} is the permittivity for dielectric displacement and electric field in direction 3 (parallel to direction in which ceramic element is polarized), under constant strain (Piezoelectric ceramics properties & applications, n.d.).

A dielectric, or electrical insulator, is a substance that is highly resistant to flow of electric current, and has a relative permittivity greater than unity. In a perfect dielectric, the voltage wave and the current are exactly 90° out of phase. As the dielectric becomes less than 100% efficient, the current wave begins to lag the voltage in direct proportion. The amount the current wave deviates from being 90° out of phase with the voltage is defined as the dielectric loss angle. The tangent of this angle is known as the loss tangent or dissipation factor (Barsoum, 1997).

In case of ac field, the dielectric constant has both a real part and an imaginary part; the loss tangent is defined as the ratio of the imaginary part to the real part. The dielectric constant (ε_r) and dielectric loss factor (tan δ) can be measured using a standart impedance bridge or an impedance analyzer both of which provide a direct reading (Barsoum, 1997).

2.5.1.4 Coupling Coefficients

The piezoelectric efficiency is measured in terms of a coupling coefficient. The piezoelectric coupling factor k is a measurement of the overall strength of the electromechanical effect. It is often as the square root of the ratio of electrical energy output to the total mechanical energy input (in the case of the direct effect) or the mechanical energy available to the total electrical energy (in the case of the coverse effect). The value of k is of course always less than unity because energy conversion is always incomplete (Prasad, 2005).

$$k = \sqrt{\frac{\text{mechanical energy stored}}{\text{electrical energy applied}}} \qquad (2.14)$$

or

$$k = \sqrt{\frac{\text{electrical energy stored}}{\text{mechanical energy applied}}} \qquad (2.15)$$

Subscripts denote the relative directions of the electrical and mechanical quantities and the kind of motion involved. Special cases of the coupling factor are the planar coupling factor k_p, and the thickness coupling factor k_t. The planar coupling factor kp of a thin disc represents the coupling between the electric field in direction 3 (parallel to the disc axis) and simultaneous mechanical effects in directions 1 and 2 (Figure 2.12) that result in radial vibrations. This is known as radial coupling. The thickness coupling factor kt represents the coupling between an electric field in direction 3 and the mechanical vibrations in direction 3 of a thin planar object (i.e. an object whose surface dimensions are large compared with its thickness) (Piezoelectric ceramics properties & applications, n.d.).

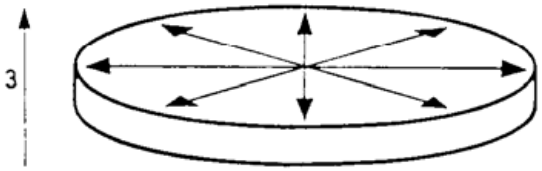

Figure 2.12 Planar oscillations of a thin disc of piezoelectric material (Piezoelectric ceramics properties & applications, n.d.).

Whereas, k_{33} is the factor for electric field in direction 3 (parallel to direction in which ceramic element is polarized) and longitudinal vibrations in direction 3 (ceramic rod, length >10x diameter). k_{31} factor for electric field in direction 3 (parallel to direction in which ceramic element is polarized) and longitudinal vibrations in direction 1 (perpendicular to direction in which ceramic element is polarized). Since these coefficients are energy ratios, they are dimensionless (Piezoelectric ceramics properties & applications, n.d.).

2.5.1.5 Young's Modulus

Young's modulus, Y, is an indicator of the stiffness (elasticity) of a ceramic material. Y is determined from the value for the stress applied to the material divided by the value for the resulting strain in the same direction (Sparkler piezoceramics, n.d.).

$$Y = (F/A)/(\Delta L/L) = T/S \qquad (2.16)$$

2.5.1.6 Elastic Compliance

Elastic compliance, s, is the strain produced in a piezoelectric material per unit of stress applied and, for the 11 and 33 directions, is the reciprocal of the modulus of elasticity (Young's modulus, Y). s^D is the compliance under a constant electric displacement; s^E is the compliance under a constant electric field. The first subscript indicates the direction of strain; the second is the direction of stress.

s_{11}^E is the elastic compliance for stress in direction 1 (perpendicular to direction in which ceramic element is polarized) and accompanying strain in direction 1, under constant electric field (short circuit). s_{33}^D elastic compliance for stress in direction 3 (parallel to direction in which ceramic element is polarized) and accompanying strain in direction 3, under constant electric displacement (open circuit) (Piezoelectric ceramics properties & applications, n.d.).

$$s_{33}^{D} = 1 / Y_{33}^{D} \qquad (2.17)$$

$$s_{33}^{E} = 1 / Y_{33}^{E} \qquad (2.18)$$

$$s_{11}^{D} = 1 / Y_{11}^{D} \qquad (2.19)$$

$$s_{11}^{E} = 1 / Y_{11}^{E} \qquad (2.20)$$

2.5.1.7 Mechanical Quality Factor

The most common method of determining the resonance properties of a piezoelecric material involves measuring the impedance of the material as a function of frequency. Electrical impedance or simply impedance is a measure of opposition to a sinusoidal electric current. When exposed to an AC electric field, a piezoelectric ceramic element changes dimensions cyclically, at the cycling frequency of the field. The frequency at which the ceramic element vibrates most readily, and most efficiently converts the electrical energy input into mechanical energy, is the resonance frequency. The pattern of an element's responses is depicted in Figure 2.13. As the cyclic frequency is increased, the element's oscillations first approach a frequency which makes impedance minimum. This minimum impedance frequency, $f_{m,}$ also is the resonance frequency, f_r. Composition of the ceramic material and the shape and volume of the element determine the resonance frequency, generally, a thicker element has a lower resonance frequency than a thinner element of the same shape (Piezoelectric impedance, 2005).

As the cycling frequency is further increased, impedance increases to a maximum. The maximum impedance frequency, f_n , also is the anti-resonance frequency, f_a. Maximum response from the element will be at a point between f_m and f_n.

A ceramic element's oscillations first approach the minimum impedance frequency (f_m) / resonance frequency (f_r), at which the element vibrates most readily,

and most efficiently converts electrical energy into mechanical energy. As cycling frequency is further increased, impedance increases to the maximum impedance frequency (f_n) / anti-resonance frequency (f_a) (Piezoelectric impedance, 2005).

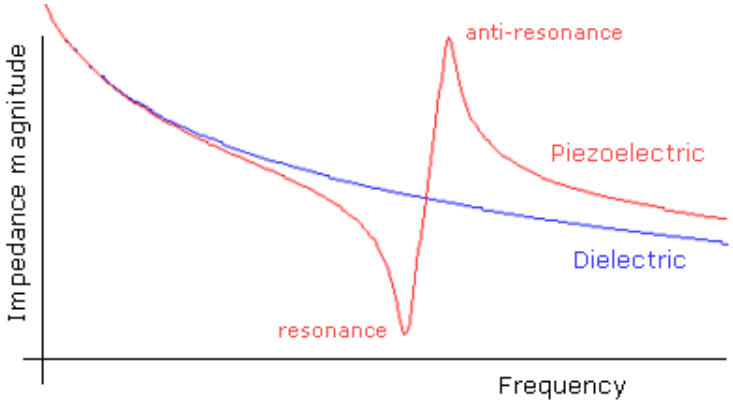

Figure 2.13 Impedance as a function of cycling frequency (Piezoelectric impedance, 2005).

The impedance for a non-piezoelectric element (of the same shape and dielectrical properties) is also shown in blue.

The resonances result from the electrical input signal exciting a mechanical resonance in the piezo element. For each mechanical resonance in the piezo element, a resonance/anti-resonance pair will exist in the impedance. The impedance of the piezoelectric material passes through a minimum at the resonance frequency and a maximum at the anti-resonance frequency. The mechanical quality factor (Q_m) is defined as the ratio of the reactance to the resistance in the series equivalent circuit representing the piezoelectric resonator. The Q_m can be used to determine the sharpness of the resonance peak.

$$Q_m = \left(\frac{1}{2\pi f_r Z_m C}\right)\left(\frac{f_a^2}{f_a^2 - f_r^2}\right) \qquad (2.21)$$

Where f_r and f_a are the resonance and anti-resonance frequency (Hz). Z_m is the impedance and C is the capacitance.

2.5.1.8 Capacitance

A capacitor is a device that stores energy in the electric field created between a pair of conductors on which equal but opposite electric charges have been placed.

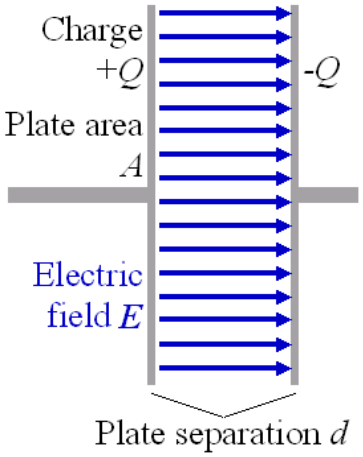

Figure 2.14 Parallel-plate capacitor (Dielectric, n.d.).

When electric charge accumulates on the plates, an electric field is created in the region between the plates that is proportional to the amount of accumulated charge. This electric field creates a potential difference V = E·d between the plates of this simple parallel-plate capacitor.

The capacitor's capacitance (C) is a measure of the amount of charge (Q) stored on each plate for a given potential difference or voltage (V) which appears between the plates (Dielectric, n.d.).

$$C = \frac{Q}{V} = \frac{coulombs}{volts} = farad \qquad (2.22)$$

The use of a dielectric in a capacitor presents several advantages. The simplest of these is that the conducting plates can be placed very close to one another without risk of contact. Also, if subjected to a very high electric field, any substance will ionize and become a conductor. Dielectrics are more resistant to ionization than air, so a capacitor containing a dielectric can be subjected to a higher voltage.

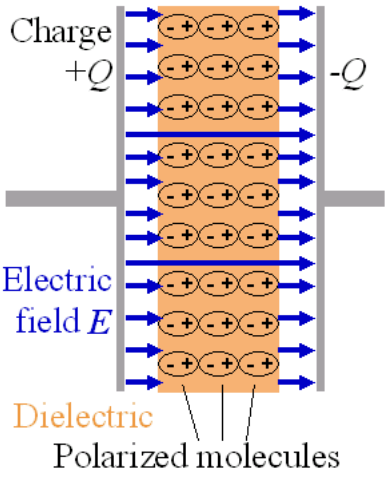

Figure 2.15 Same as (2.14) except that not a dielectric is placed between the plates (Dielectric, n.d.).

Putting a dielectric material between the plates in a parallel plate capacitor causes an increase in the capacitance in proportion to K, the dielectric constant of the material:

$$C = \frac{K.\varepsilon_0.A}{d} \qquad (2.23)$$

Where: C= capacitance, A= capacitor plate area, ε_0 = permittivity of air = 8.85×10^{-12} farads/meter, K= relative dielectric constant of the dielectric and d = distance between the plates.

At frequencies far below resonance, piezoelectric ceramic transducers are fundamentally capacitors.

2.6 Important Commercial Piezoceramics

2.6.1 Barium Titanate ($BaTiO_3$, BT)

Barium titanate is most widely used for its strong piezoelectric characteristics.The high dielectric constant of $BaTiO_3$-type ceramics results from the

crystal structure $BaTiO_3$ has the perovskite structure, as illustrated in Figure 2.16. Each barium ion is surrounded by 12 oxygen ions. The oxygen ions plus the barium ions form a face-centered cubic lattice. The titanium atoms reside in octahedral interstitial positions surronded by six oxygen ions. Because of the large size of the Ba ions, the octahedral interstitial position in $BaTiO_3$ is quite large compared to the size of the Ti ions. The Ti ions are on the magrin of being too small to be stable in this octahedral position. It is belived that there are minimum-energy positions off-center in the direction of each of the six oxygen ions surrounding the Ti ion. This results in spontaneous polarization for each Ti ion. Since each Ti ion has a +4 charge, the degree of polarization is very high. When an electric field is applied, the titaniun ions can shift from random to aligned positions and result in high bulk polarization and high dielectric constant, but they return to its stable central position as soon as the field is removed. Thus, there is no retained polarization, no hysteresis loop, and no ferroelectric behaviour has a cubic structure and is not ferroelectric (Richerson, 1992).

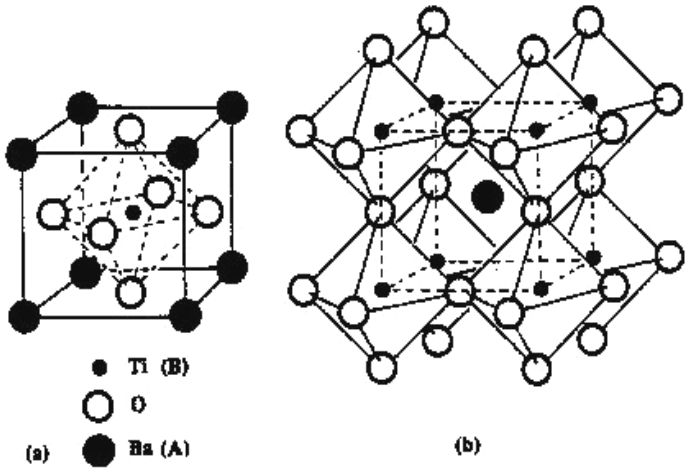

Figure 2.16 (a) A cubic ABO_3 ($BaTiO_3$) perovskite-type unit cell and (b) three dimensional network of corner sharing octahedra of O^{2-} ions (Safari et al., n.d.).

Temperature has a strong effect on the crystal structure and polarization characteristics of $BaTiO_3$ as shown in Figure 2.17. Above its Curie point of about 130 °C, Barium titanate ($BaTiO_3$) has a paraelectric cubic phase and the behaviour described above prevails. The thermal vibration is high enough to result in the random orientation of the titanium ions (Safari et al., n.d.).

As the temperature of $BaTiO_3$ is lowered slightly below 130 °C, one crystallographic axis increases in length (unit cell goes from 4.010 to 4.022 °A) and the other two decrease in length (4.010 to 4.004 °A). The Ti^{4+} ion moves off-center toward one of the two oxygen ions of the long axis, resulting in a spontaneous increase in positive charge in this direction. This results in a permanent electrical dipole during the initial transformation of a crystal from cubic to tetragonal. All Ti^{4+} ions do not shift in the same direction. In fact, each Ti^{4+} ion has an equal probability of shifting in six directions toward one of the corners of the octahedron. As a result, the tetragonal crystal contains ordered dipoles are giving a domain structure. (Richerson, 1992)

Application of an electric field opposite to the polarity of this original dipole will cause the Ti^{4+} ion to move through the center of the octahedral site and to an equivalent off-center position. This results in a reversal in polarization, hysteresis in the *E* versus *P* curve, and ferroelectricity.

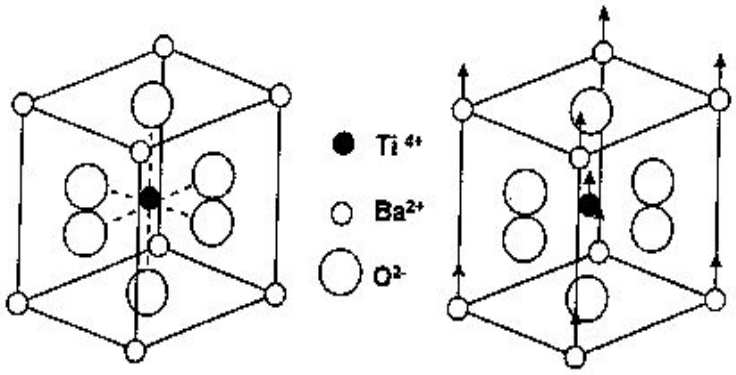

Figure 2.17 The crystal structure of $BaTiO_3$ (a) above the Curie point the cell is cubic; (b) below the Curie point the structure is tetragonal with Ba^{2+} and Ti^{4+} ions displaced relative to O^{2-} ions (Safari et al., n.d.).

Between 0 ^oC and -90 ^oC, the ferroelectric orthorhombic phase is stable, on decreasing the temperature below -90 ^oC the phase transition from the orthorhombic to ferroelectric rhombohedral phase occurs (Safari et al., n.d.).

Barium titanate, like other asymmetrical crystals, develops a potential difference when compressed in specific crystallographic directions. Similarly, the application of

an electric voltage creates a mechanical distortion. This arises from the anisotropic nature of the dielectric characteristics. In practice, polycrystalline barium titanate piezoelectrics are made by cooling through the Curie temperature in the presence of a strong electric field which gives permanent orientation of the dipoles in the ceramic rather than the random arrangement which would otherwise occur.

The polarization characteristics can be modified by crystal chemical alterations of the crystal structure. Various A and B site substitutions in different concentrations have been tried to see their effect on the dielectric and ferroelectric properties of $BaTiO_3$. Substitutions also modify the temperature effect. Additions to $BaTiO_3$ of $CaZrO_3$ and $MgZrO_3$ results in a decrease in sensitivity to temperature by broadening the temperature versus K´ curve. Additions of $SrTiO_3$, $SrSnO_3$, $CaSnO_3$ or $BaSnO_3$ reduce the Curie temperature. Addition to $BaTiO_3$ of $PbTiO_3$ with a higher Curie temperature increases Curie temperature and at which the dielectric constant is a maximum (Kingery at al, 1976).

The dielectric properties of $BaTiO_3$ are found to be dependent on the grain size. Figure 2.18 shows the variation of dielectric constant with temperature for $BaTiO_3$ ceramics with a fine (~ 1 μm) and coarse (~ 50 μm) grain size. Large grained $BaTiO_3$ shows an extremely high dielectric constant at the Curie point. This is because of the formation of multiple domains in a single grain, the motion of whose walls increases the dielectric constant at the Curie point. For a $BaTiO_3$ ceramic with fine grains (~ 1 μm), a single domain forms inside each grain. The movement of domain walls is restricted by the grain boundaries, thus leading to a low dielectric constant at the Curie point as compared to coarse grained $BaTiO_3$. The room temperature dielectric constant (ε_r) of coarse grained (≥ 10 μm) BT ceramics is found to be in the range of 1500-2000. On the other hand, fine grained (~1 μm) BT ceramics exhibit a room temperature dielectric constant between 3500-6000. The grain size effect on the dielectric constant at room temperature has been explained by the work of Buessem et al. and Arlt et al. (Safari et al., n.d.). Buessem and coworkers proposed that the internal stresses in fine grained $BaTiO_3$ must be much greater than the coarse grained ceramic, thus leading to a higher permittivity at room temperature (Safari et al., n.d.).

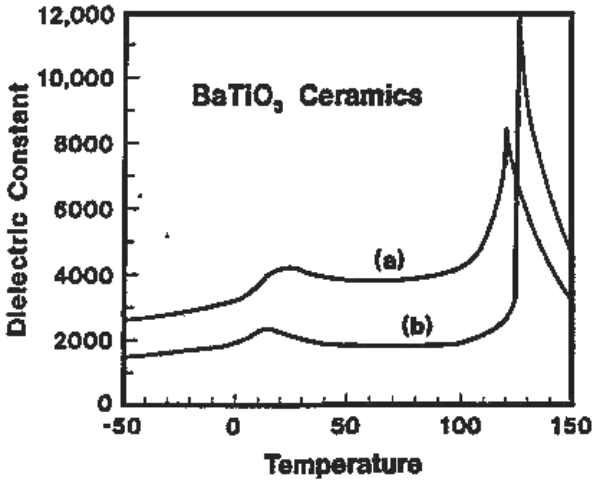

Figure 2.18 The variation of the relative permittivity (ε_r) with temperature for $BaTiO_3$ ceramics with (a) 1 μm grain size and (b) 50 μm grain size (Safari et al., n.d.).

As the BT ceramics have a very large room temperature dielectric constant, they are mainly used multilayer capacitor applications. The grain size control is very important for these applications.

Barium titanate prepolarized ceramics have the advantage of a high coupling coefficient (approximately 0.5 as compared with a value of 0.1 for quartz and other useful piezoelectrics), and at the same time they are mechanically and thermally stable. Barium titanate can be manufactured in a variety of shapes and subsequently polarezed in order to obtain optimum efficiency as piezoelectric elements. Since the Crue temperature of barium titanate is relatively high, piezoelectric properties are maintained, and barium titanate can be used for these puposes, at temperatures as high as 70^{o}C (Kingery et al., 1976).

Transducers of barium titanate are widely used for ultrasonic technical applications such as the emulsification of liquids, mixing of powders and paints, and homogenization of milk; they are also used in microphones, phonography pickups, accelerometers, strain gauges, and sonar devices (Kingery et al., 1976).

2.6.2 Lead Titanate ($PbTiO_3$, PT)

Lead titanate is a ferroelectric material having a structure similar to $BaTiO_3$ with a high Curie point (490 ^oC). On decreasing the temperature through the Curie point a phase transition from the paraelectric cubic phase to the ferroelectric tetragonal phase takes place (Safari et al., n.d.).

Lead titanate ceramics are difficult to fabricate in the bulk form as they undergo a large volume change on cooling below the Curie point. It is the result of a cubic (c/a = 1.00) to tetragonal (c/a = 1.064) phase transformation leading to a strain of > 6%. Hence, pure $PbTiO_3$ ceramics crack and fracture during fabrication. The spontaneous strain developed during cooling can be reduced by modifying the lead titanate with various dopants such as Ca, Sr, Ba, Sn, and W to obtain a crack free ceramic.

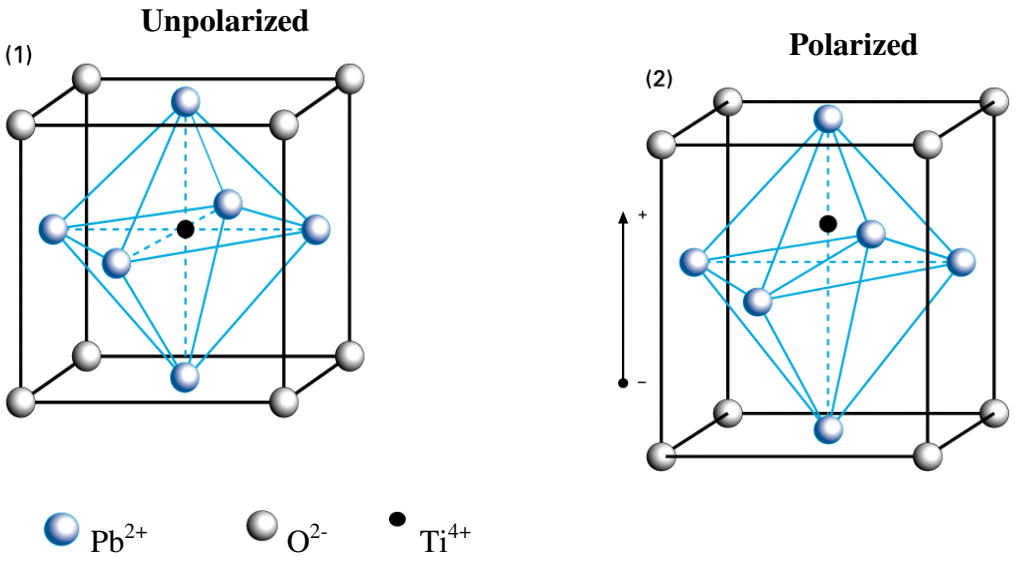

Figure 2.19 Crystal structure of a $PbTiO_3$; (1) temperature above Curie point, (2) temperature belove Curie point.

2.6.3 Lead Zirconate Titanate [$Pb(Zr_xTi_{1-x})O_3$, PZT]

Lead Zirconate Titanate (PZT) is a binary solid solution of $PbZrO_3$ an antiferroelectric (orthorhombic structure) and $PbTiO_3$ a ferroelectric (tetragonal

perovskite structure). PZT has a perovskite type structure with the Ti^{4+} and Zr^{4+} ions occupying the B site at random.

The PZT phase diagram is shown in Figure 2.20. At high temperatures PZT has the cubic perovskite structure which is paraelectric. On cooling below the Curie point line, the structure undergoes a phase transition to form a ferroelectric tetragonal or rhombohedral phase. In the tetragonal phase, the spontaneous polarization is along the <100> set of directions while in the rhombohedral phase the polarization is along the <111> set of directions. The MPB separating the two ferroelectric tetragonal and orthorhombic phases has a room temperature composition with a Zr/Ti ratio of ~ 52/48. PZT ceramics with the MPB composition show excellent piezoelectric properties (Safari et al., n.d.).

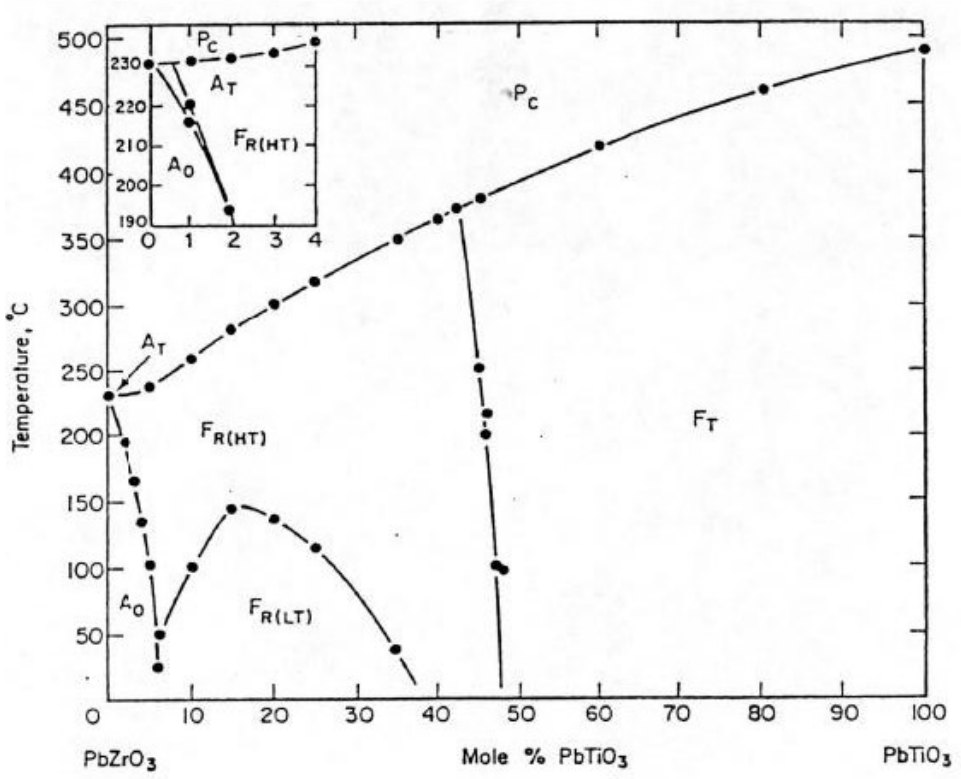

Figure 2.20 The PZT phase diagram (Safari et al., n.d.).

At compositions near the MPB the coupling coefficient and the relative permittivity peak, as shown in Figure 2.28 (Safari et al., n.d.).

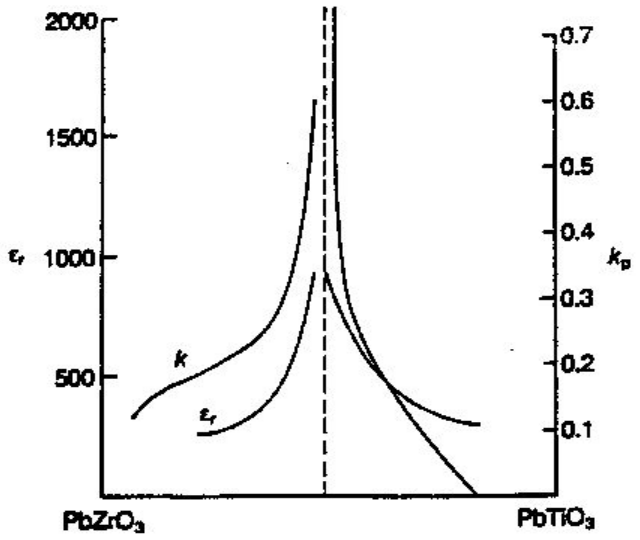

Figure 2.21 The effect of composition on the dielectric constant and electromechanical coupling factor k_p in PZT ceramics (Safari et al., n.d.).

The poling of the PZT ceramic is also easy at this composition because the spontaneous polarization within each grain can be switched to one of the 14 possible orientations (eight [111] directions for the rhombohedral phase and six [100] directions for the tetragonal phase). Below the Zr/Ti ratio of 95/5 the solid solution is antiferroelectric with an orthorhombic phase. On the application of an electric field to this composition a double hysteresis loop is obtained. This is because of the strong influence of the antiferroelectric $PbZrO_3$ phase (Safari et al., n.d.).

In order to suit some specific requirements for certain applications, piezoelectric ceramics can be modified by doping them with ions which have a valence different than the ions in the lattice. Piezoelectric PZT ceramics having the composition at the MPB can be doped with ions to form "soft" and "hard" PZT's. Soft PZT's are doped with donor ions, i.e. dopants of higher charge than that of the replaced ions, such as La^{3+} (for A site) and Nb^{5+}, Sb^{5+} (for B site) leading to the creation of A site vacancies in the lattice. Donor-doped PZTs have higher permittivities, larger losses, and higher piezoelectric coefficient and are easy to pole and depole. Therefore more suitable for converting mechanical into electrical vibrations. They can be used for applications requiring very high piezoelectric properties (Safari et al., n.d.). Soft ceramics

produce larger displacements and wider signal band widths, relative to hard ceramics, but they exhibit greater hysteresis, and are more susceptible to depolarization or other deterioration. Lower Curie points (generally below 300 °C) dictate that soft ceramics be used at lower temperatures. Generally large values for permittivity and dielectric dissipation factor restrict or eliminate soft ceramics from applications requiring combinations of high frequency inputs and high electric fields. Consequently, soft ceramics are used primarily in sensing applications, rather than in power applications.

On the other hand, hard PZT's are doped with acceptor ions such as K^+, Na^+ (for A site) and Fe^{3+}, Al^{3+}, Mn^{3+} (for B site), creating oxygen vacancies in the lattice. Hard PZT's have characteristics generally opposite those of soft ceramics, including Curie points above 300 °C, lower permittivities, smaller electrical losses, small piezoelectric charge constants, large electromechanical coupling factors, and large mechanical quality factors. These are more difficult to polarize or depolarize, thus making them ideal for rugged applications. Although hard ceramics generally are more stable than soft ceramics, they cannot produce the same large displacements. Hard ceramics are compatible with high mechanical loads and high voltages.

Table 2.1 Common aliovalent substituents in perovskite type ceramics (Moulson et al., 1990).

A-site donors	La^{3+}, Bi^{3+}, Nd^{3+}
B-site donors	Nb^{5+}, Ta^{5+}, Sb^{5+}
A-site acceptors	K^+, Rb^+
B-site acceptors	Co^{3+}, Fe^{3+}, Sc^{3+}, Ga^{3+}, Cr^{3+}, Mn^{3+}, Mn^{2+}, Mg^{2+}, Cu^{2+}

Some applications require low mechanical as well as low dielectric losses combined with piezoelectric activity. This seems to be best achieved by substituting mixture of B-site donors and acceptors such as Nb and Mg in 2:1 atomic proportions.

Be aware, however, that a soft ceramic can be prepared to exhibit some characteristics approaching those of a hard ceramic, or vice versa. Thus, when choosing a ceramic for a particular application, it can be useful to look beyond

general categorization, and carefully compare specific characteristics (Piezo theory, 1998).

Table 2.2 Characteristics of soft ceramics and hard ceramics compared (Piezo theory, 1998).

Characteristic	**Soft Ceramic**	**Hard Ceramic**
Piezoelectric Constants	larger	smaller
Permittivity	higher	lower
Dielectric Constants	larger	smaller
Dielectric Losses	higher	lower
ElectromechanicalCoupling Factors	larger	smaller
Electrical Resistance	very high	lower
Mechanical Quality Factors	low	high
Coercive Field	low	higher
Polarization / Depolarization	easier	more difficult

2.7 Applications

A piezoelectric system can be constructed for virtually any application for which any other type of electromechanical transducer can be used. For any particular application, however, limiting factors include the size, weight, and cost of the system. Piezoceramic devices fit into five general categories: generators, sensors, actuators, transducers, and transformers. Characteristics of each group are briefly summarized here (Piezo theory, 1998).

2.7.1 Generators

Piezoelectric ceramics can generate voltages sufficient to spark across an electrode gap, and thus can be used as ignitors in fuel lighters, gas stoves, welding equipment, and other such apparatus. Piezoelectric ignition systems are small and simple, distinct advantages relative to alternative systems that include permanent magnets or high voltage transformers and capacitors (Piezo theory, 1998).

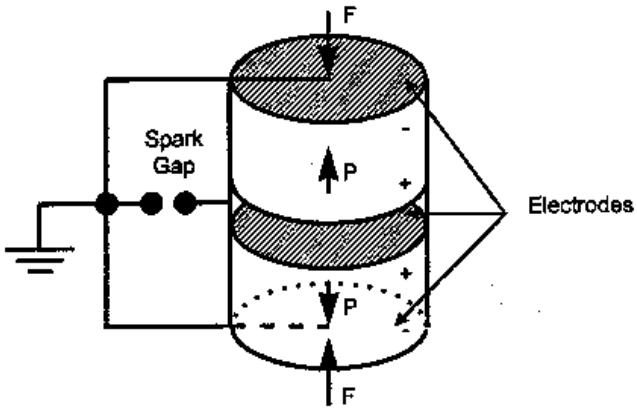

Figure 2.22 A piezoelectric spark generator (Piezo theory, 1998).

The principle of a gas igniter is illustrated in Figure 2.29. It is usual to use two poled cylinders back to back, rather than one, so as to have twice the charge available for the spark. It is necessary t to apply the force F quickly otherwise the voltage generated disappears as charge leaks away through the piezoceramic, across its surfaces and via the apparatus (Moulson et al., 1990).

Alternatively, the electrical energy generated by a piezoelectric element can be stored. Techniques used to make multilayer capacitors have been used to construct multilayer piezoelectric generators. Such generators are excellent solid state batteries for electronic circuits (Piezo theory, 1998).

2.7.2 Sensors

A sensor converts a physical parameter, such as acceleration or pressure, into an electrical signal. In some sensors the physical parameter acts directly on the piezoelectric element; in other devices an acoustical signal establishes vibrations in the element and the vibrations are, in turn, converted into an electrical signal. Often, the system provides a visual, audible, or physical response to the input from the sensor such as automobile seatbelts lock in response to a rapid deceleration (Piezo theory, 1998).

When force is applied to a long piezoelectric cantilever beam, one side is in tension while the other side will be in compression. No electrical output can be obtained from this homogenous body by bending. Bimorphs made with two halves of separate beams with an electrode in between as well as on the top and bottom surfaces is shown in Figure 2.23. If the beams are poled in the opposite direction then on the application of a force 'F' the voltage generated on the outer electrodes will be additive (Figure 2.23(a)). If the beams are poled in the same direction, the additive output can be obtained by connecting the outer electrodes and the center electrode as shown in Figure 2.23(b) (Safari et al., n.d.).

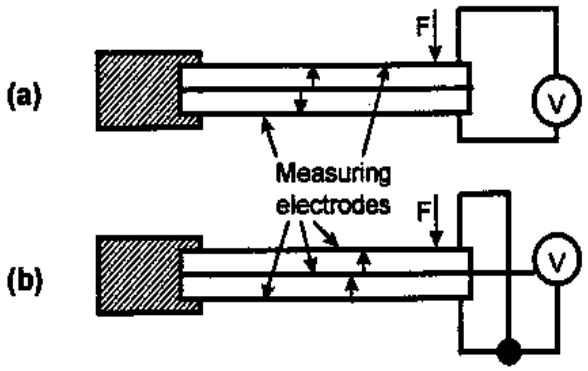

Figure 2.23 Cantilever bimorphs with (a) a series connection and (b) parallel connection of beams (Safari et al., n.d.).

2.7.3 Actuators

A piezoelectric actuator converts an electrical signal into a precisely controlled physical displacement, to finely adjust precision machining tools, lenses, or mirrors. Piezoelectric actuators also are used to control hydraulic valves, act as small-volume pumps or special-purpose motors, and in other applications. Piezoelectric motors are unaffected by energy efficiency losses that limit the miniaturization of electromagnetic motors, and have been constructed to sizes of less than 1 cm^3. A potentially important additional advantage to piezoelectric motors is the absence of electromagnetic noise (Piezo theory, 1998).

Alternatively, if physical displacement is prevented, an actuator will develop a useable force.

Dot matrix impact printers driven by multilayer piezoelectric ceramic actuators have been successfully produced on a large commercial scale. As shown in Figure 2.24, the printing pin element consists of a piezoactuator, a stroke amplifier operated on the lever principle and a printing wire. When a pulse with a peak voltage of 150 V is applied to the piezoelectric actuator, the printing wire moves by about 400 μm, making the tip of the wire to hit the paper through the ink ribbon. The advantages of the dot matrix printer over the conventional electromagnetic drive printers includes a higher printing speed (double the speed because of the presence of 24 printing pin elements) and half the power consumption as compared to the latter printer (Safari et al., n.d.).

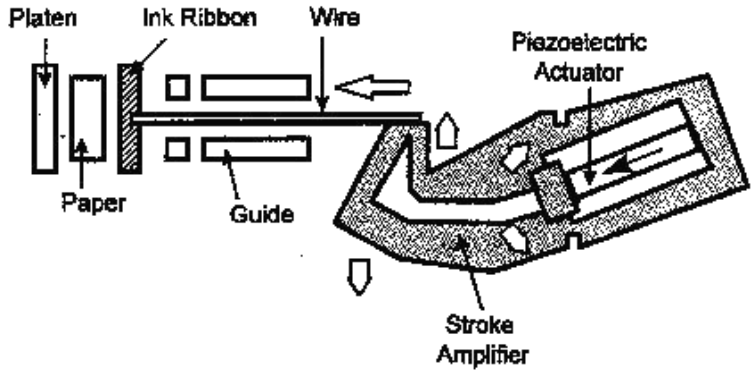

Figure 2.24 Schematic of a printing pin element (Safari et al., n.d.).

2.7.4 Transducers

Piezoelectric transducers convert electrical energy into vibrational mechanical energy, often sound or ultrasound, which is used to perform a task. Piezoelectric transducers that generate audible sounds afford significant advantages, relative to alternative electromagnetic devices as they are compact, simple, and highly reliable, and minimal energy can produce a high level of sound. These characteristics are ideally matched to the needs of battery-powered equipment (Piezo theory, 1998).

Because the piezoelectric effect is reversible, a transducer can both generate an ultrasound signal from electrical energy and convert incoming sound into an

electrical signal. Some devices designed for measuring distances, flow rates, or fluid levels incorporate a single piezoelectric transducer in the signal sending and receiving roles, other designs incorporate two transducers and separate these roles.

Piezoelectric transducers also are used to generate ultrasonic vibrations for cleaning, atomizing liquids, drilling or milling ceramics or other difficult materials, welding plastics, medical diagnostics, or for other purposes.

2.7.5 Piezoelectric Transformers

The transfer of energy from one set of electrodes to another on a ceramic body can be used for voltage transformation. Piezoelectric transformers have an analogous operating mechanism to magnetic devices for converting voltage. Whereas a magnetic transformer operates by converting an electrical input to magnetic energy and then reconverting the magnetic energy back to an electrical output, piezoelectric transformers convert an electrical input into mechanical energy and subsequently reconvert this mechanical energy back to an electrical output (Actuators, generators, sensors, transformers, & transducers, n.d.).

The input signal causes the piezoelectric transformer to vibrate at the resonant frequency of the component. The secondary side of the transformer acts as a piezo generator, generating the transformed voltage (Actuators, generators, sensors, transformers, & transducers, n.d.).

Low voltage to high voltage transformation can be done by using a piezoelectric plate. Figure 2.25 shows a flat plate having electrodes on half of it larger face and on an edge. The region between the larger face electrodes and the edge electrode are poled separately. A length mode resonance is excited by applying a low AC voltage source between the larger face electrodes. The step up voltage ration would be proportional to the ratio of the input to output capacitance and the efficiency of the device. This principle has been used for making EHT transformers for miniature television receivers (Safari et al., n.d.).

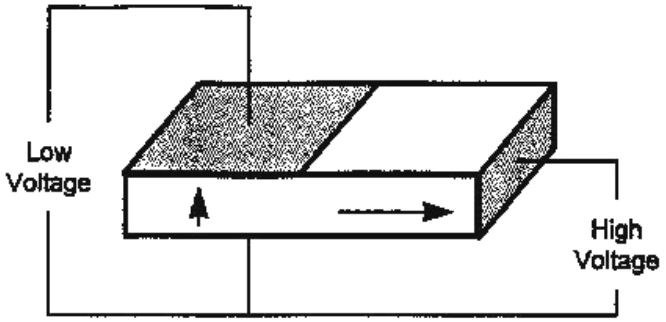

Figure 2.25 Piezoelectric transformers with the arrows indicating the poling directions (Safari et al., n.d.).

CHAPTER THREE
SOL-GEL PROCESSING

The general principle involved in the solution deposition of perovskite films is to prepare a "homogeneous" solution of the necessary cation species that may later be applied to a substrate. The fabrication of thin films by this approach involves four basic steps: (i) synthesis of the precursor solution, (ii) deposition by spin-casting or dip-coating, where drying processes usually begin depending on the solvent, (iii) low-temperature heat treatment for drying, pyrolysis of organic species (typically 300-400 °C), and formation of an amorphous film, and (iv) higher temperature heat treatment for densification and crystallization of the coating into the desired oxide phase (600-1100 °C) (Schwartz, 1997).

A sol is a stable suspension of colloidal solid particles within a liquid. For a sol to exist, the solid particles, denser than the surrounding liquid, must be small enough for the forces responsible of dispersion to be greater than those of gravity. The solvent used to disperse stably the colloidal particles of a sol is often either pure water or a solution composed mostly of water. However, other solvents such as alcohol can also be used (Pierre, 1998).

A gel is a porous 3-dimensionally interconnected solid network that expands in a stable fashion throughout a liquid medium and is only limited by the size of the container. If the solid network is made of colloidal sol particles the gel is said to be colloidal. If the solid network is made of sub-colloidal chemical units then the gel is polymeric. A polymer, as defined by Flory, is a group of molecules whose structure can be generated through repetition of one or a few elementary units (Pierre, 1998).

The nature of gels depends on the coexistence between the solid network and the liquid medium. If the liquid is mostly composed of water, and if that aqueous phase is the one present in greatest proportion, then the corresponding gel is an aquagel (or hydrogel). If the liquid phase is largely composed of an alcohol then the gel is an alcogel. Finally, if most of the liquid is removed, then the brittle solid obtained is

either called a xerogel or an aerogel, depending on the drying method (they can also be called more simply dry gels) (Pierre, 1998).

A gel forms when the homogenous dispersion present in the initial sol rigidifies. This process, called gelation, prevents the development of inhomogeneities within the material. A sol, or a solution, can be transformed into a colloidal (or polymeric) gel by going through what is called a gel-point. Practically, it is at this point that the sol suddenly changes from a viscous liquid state to a solid phase called the gel (Pierre, 1998).

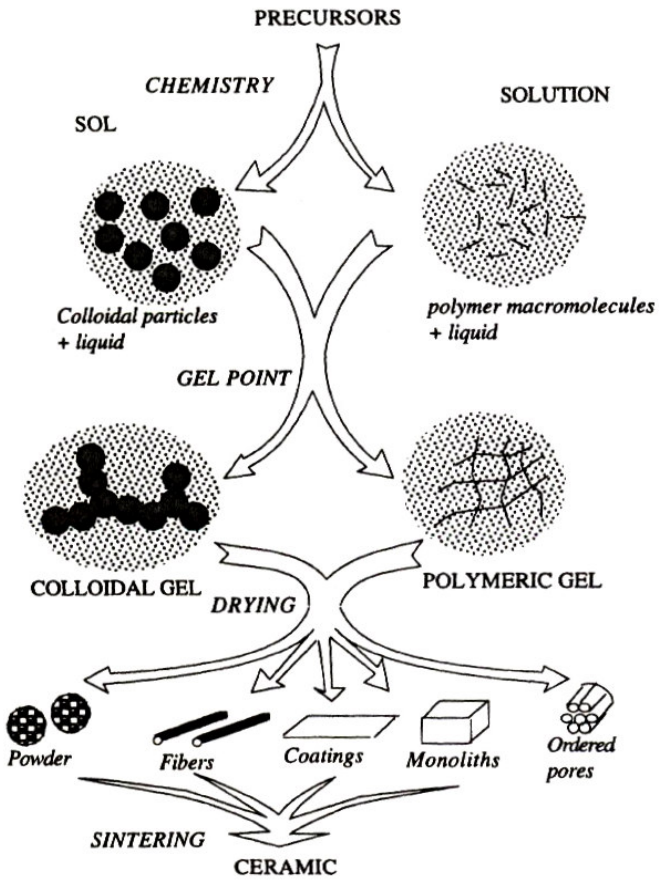

Figure 3.1 Simplified chart of sol-gel process (Pierre, 1998).

3.1 Solution Preparation

Solution preparation of perovskite materials generally involves the use of chemical reactants that are dissolved in a common solvent. The chemical reactant which contains the cation M (metal) present in the final inorganic sol or gel is called the chemical precursor. The starting reagents (precursors) are typically the metallic salts and the alkoxides. The general formula of a metallic salt is M_mX_n where M is the metal, X an anionic group, and m and n stoichiometric coefficients. As for alkoxides, their general formula is $M(OR)_n$, which indicates that they are a combination of a cation M with n alcohol groups ROH. Since the solution chemistry of these two groups are quite different, the choice of the solvent as either water or an organic liquid depends on the precursor. The solution route used will also determine the extent of intermixing of the metal species, whether formation of a network versus formation of individual inorganic phases occurs, the carbon content of the films, the temperature at which pyrolysis of organic species occurs, the weight loss associated with oxide formation, the densification and crystallization behavior of the film, and stress development within the film. While some of these effects are now well understood, others are less clear, partly because of the difficulty in characterizing the solution precursor and the resulting amorphous film. For thin film production, metal alkoxides are better than its salts as a precursor to achieve crack-free, pinhole-free, homogeneous and textured films. In addition to precursor characteristics, film processing behavior, such as substrate wetting, can also play a role in determining the solution chemistry that must be developed. Film properties that can necessitate changes in solution chemistry include poor thickness uniformity, crack formation, crystallization behavior and phase purity, and compositional nonuniformities (Pierre, 1998).

Solvents characterized both by a permanent dipole moment μ and by a relative dielectric constant ε_r. A high relative dielectric constant (ε_r>40) is often due to the existence of a permanent dipole moment. Such molecules have good ionizing properties and can therefore dissolve other polar solute. On the other hand when the

solvent's relative constant is low (ε_r<20), it has a weak ionizing property and can only dissolve less polar solute (Pierre, 1998).

Organic solvents are frequently used in sol-gel processing as they allow the control of the reaction of alkoxide precursors with water, and hence to direct with more flexibility the structure of sol-gel products (Schwartz, 1997).

Sol-gel precursors undergo chemical reactions with solvent and the other species present in the solution. One of the most efficient models used to predict those reactions is the Partial Charge Model. Various atomic or molecular groups called ligands can bind to a complex C or cation M either directly or by substituting another ligand. The mechanism of the transformation depends on the partial charge of the different atoms in the species. Those with a negative partial charge are nucleophilic, and those with a positive charge are electrophilic. Similarly, in a substitution reaction, the new ligand with the highest partial negative charge is the nucleophile while the group in the metal complex with the highest positive charge is the leaving group. Chelating ligands also have an important effect as they are polydentate and can therefore bind to a metal atom by several bonds (Pierre, 1998).

3.2 Alkoxides Solutions

Alkoxides, also called alcoholates, are compounds with chemical formula $M(OR)_Z$ that are the result of direct or indirect reactions between a metal M and an alcohol ROH (Pierre, 1998).

When the alkoxides are dissolved in their corresponding parent alcohol, they build stable coordination complexes with the solvent. The key reactions leading to the formation of the precursor species are hydrolysis and condensation of the alkoxide reagents, in which metal-oxygen-metal (M-O-M) bonds are formed (Schwartz, 1997).

Hydrolysis:

$$M(OR)_X + H_2O \rightarrow M(OR)_{X-1}(OH) + ROH \quad (3.1)$$

Condensation (alcohol elimination):

$$2M(OR)_{X-1}(OH) \rightarrow M_2O(OR)_{2X-3}(OH) + ROH \quad (3.2)$$

Condensation (water elimination):

$$2M(OR)_{X-1}(OH) \rightarrow M_2O(OR)_{2X-2} + H_2O \quad (3.3)$$

3.2.1 Hydrolysis

Hydrolysis is the deprotonation of a solvated M cation and it consists in the loss of a proton by one or more of the water molecules that surrounds the M during hydrolysis process. As a consequence, the aqua ligand molecule, H_2O that is bonded to the metal is either transformed into a hydroxo ligand, OH^-, if only one proton leaves, or into an oxo ligand O^{-2}, if two protons separates. In alkoxides hydrolysis process, the alkoxy groups (OR) are replaced either by hydroxo ligands (OH) or oxo ligands (O) (Pierre, 1998).

This reaction is influenced by various factors including,

1. the nature of the alkyl group,
2. the nature of the solvent,
3. the concentration of each specie in the solvent,
4. the water to alkoxide molar ratio and the temperature.

In the first hydrolysis reaction, reaction (3.4), a first hydroxo ligand substitutes an alkoxy group.

$$M(OR)_Z + H_2O \Rightarrow M(OH)(OR)_{Z-1} + ROH \quad (3.4)$$

The mechanism of hydrolysis, illustrated in equation (3.5), consists in a nucleophilic substitution in which a water molecule attacks the alkoxide. It is independent of the polymerization of the alcoholate.

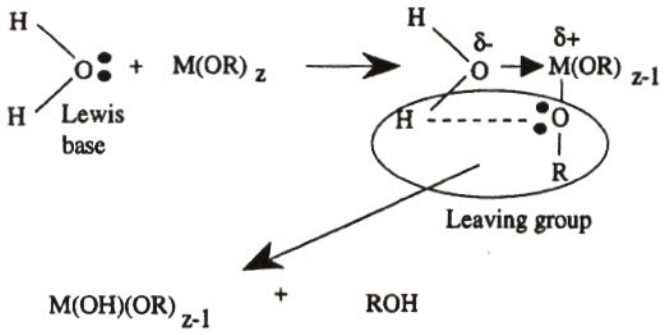

(3.5)

According to the partial charge model, an alkoxide with formula $M(OR)_Z$ undergoes hydrolysis if

a. The metal M is an electrophile ($\delta(M)>0$).
b. The oxygen is a nucleophile ($\delta(O)<0$).

A part of the complex, called the leaving group, can attain a positive partial charge thus enabling it to leave the intermediate structure. In most cases, this leaving group is either an alcohol (ROH with $\delta(ROH)>0$) or a water molecule (with $\delta(H_2O)>0$) (Pierre, 1998).

Table 3.1 Partial charge δ(M) of the metal M in a few alkoxides (Pierre, 1998).

Alkoxide	δ(M)
$Zr(OEt)_4$	**+0,65**
$Ti(OEt)_4$	**+0.63**
$VO(OEt)_4$	**+0.46**
$Si(OEt)_4$	**+0.32**

You will note from those data that the partial charge of Si in $Si(OEt)_4$ is smaller than that of the other metals in their corresponding alcoholates. It is therefore much more difficult kinetically to hydrolyze the silicium alkoxides than the others one.

For tetravalent metal alkoxides $M(OR)_4$, a more simple reactivity criterium than the cation partial charge is its unsaturation (N-z) where N is the usual coordination number of the metal M in compounds and z the formal electric charge of the corresponding cation. The value of (N-z) increases from Si to Ce as shown in Table 3.2. Hence the hydrolysis reactivity increases in order of cations Si<< Sn<Ti<Zr<Ce (Pierre, 1998).

Table 3.2 Unsaturation of tetravalent metals in alkoxides (Pierre, 1998).

Cation	N	N-z
Si	**4**	**0**
Sn	**6**	**2**
Ti	**6**	**2**
Zr	**7**	**3**
Ce	**8**	**6**

Moreover the alkoxides of alkaline and alkaline-earth elements react violently to the slightest humidity. It is therefore safer to dissolve them in appropriate solvents such as, for instance, in propanol for the propoxides.

It was also indicated by Mazdiyasni et al. (Schwartz, 1997) that traces of water vapor can also hydrolyze metal alkoxides thus transforming them into oxi-alkoxides. Such a hydrolysis follows a reaction of the type (3.6).

$$M(OR)_4 + H_2O \Rightarrow MO(OR)_2 + 2ROH \qquad (3.6)$$

3.2.2 Condensation

After hydrolysis, condensation reaction occurs to form a polynuclear complex. Condensation, in aqueous solutions, is the result of either an olation or an oxolation reaction. In either case, one must be quite careful as the oxygen present sometimes speeds the reaction to a point where it becomes necessary to work in the neutral atmosphere of argon in order to control it (Pierre, 1998).

Condensation by olation fallows nucleophilic substitution mechanism in two steps of which the first one always consist in a nucleophilic addition. It is only in the second step that the leaving group separates from the complex. This leaving group is either an alcohol molecule coming from a protonated alkoxy ligand, as in first reaction (3.7), or a water molecule coming from a solvated alkoxide, as in second reaction (3.8) (Pierre, 1998).

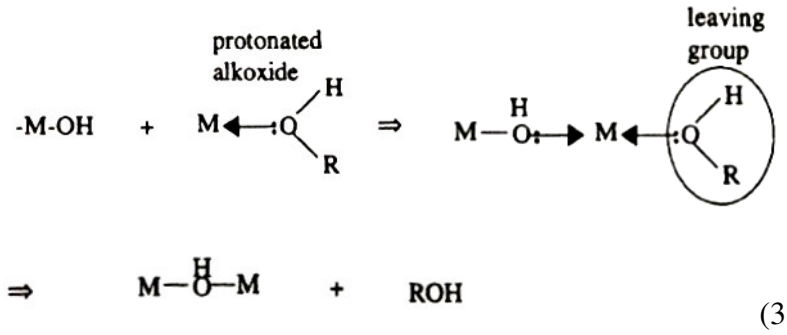

(3.7)

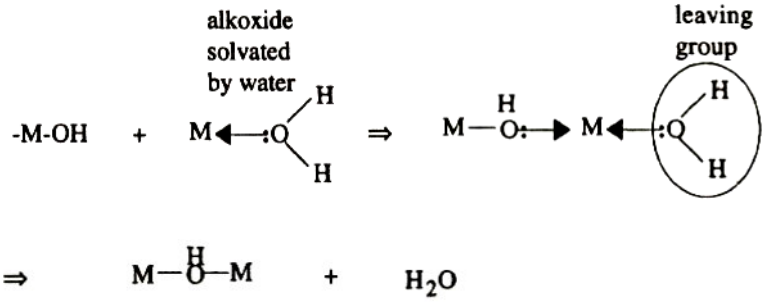

(3.8)

In the case of a departing alcohol, the protonation of the alkoxy ligand is first established by Reaction 3.9 using an acid catalysis (Pierre, 1998).

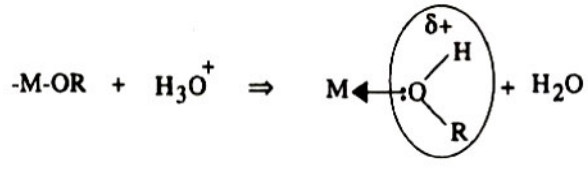

(3.9)

In the condensation by oxolation of an alkoxide, an “ol” bridge must first be established before eventually transforming into an “oxo” one. Once this “ol” bridge has been built, its corresponding hydrogen needs only to transfer either to a terminal

alkoxy ligand or to a hydroxo ligand to form the “oxo” one. In the first case, transfer of the H to an OR ligand according to Reaction (3.10), condensation is more specifically referred to as alcoxolation (Pierre, 1998).

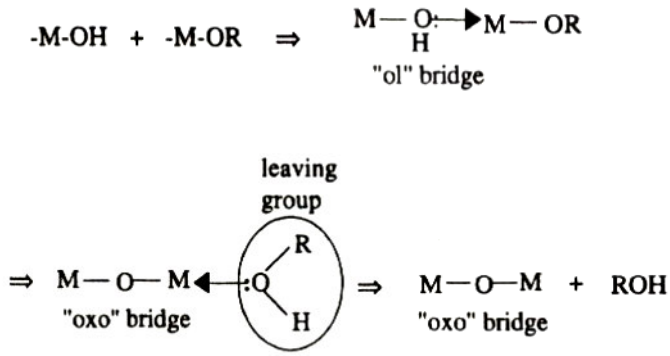

(3.10)

In the second case, transfer of the H to an OH group according to reaction (3.11), condensation is simply called oxolation (Pierre, 1998).

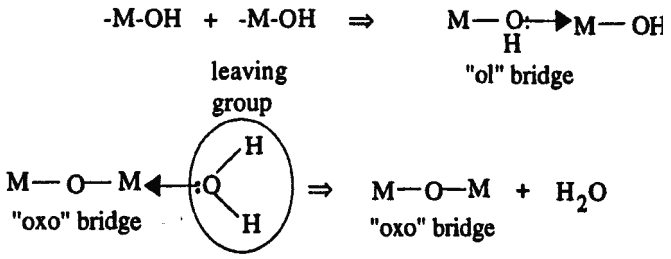

(3.11)

Oxolation can also be the result of a de-etheration as in reaction (3.12) (Pierre, 1998).

$$\text{-M-OR + RO-M- } \Rightarrow \text{ -M-O-M- + ROR} \qquad (3.12)$$

3.2.3 Precursor Mixing

Sol-gel processing offer the amazing possibility to synthesize complex oxides such as the titanate $PbTiO_3$ by mixing several oxide precursors. Those complex oxides can be established by mixing, after having previously and separately produced them by hydrolysis, the different solutions containing each a metal precursor. This

method is therefore quite similar to the conventional technique, the size of the particles or polymers present in the sol-gel stay within the colloidal range thus making the solution much more homogeneous. Lastly, in order to obtain a good interdiffusion of the metals within the product, it is necessary to heat the sol-gel at rather high temperatures (Pierre, 1998).

In most cases, when two or more simple alkoxides are mixed together in an organic solvent, they immediately attach to one another by metaloxane bonds. Titanates such as $PbTiO_3$ and $BaTiO_3$ are synthesized from an initial solution of Ti isopropoxide and Pb or Ba amyloxide refluxed in either isopropanol or benzene (Schwartz, 1997).

During solution synthesis, the chemical interactions that take place between the starting reagents will depend on both the reactivity of the compound and the solution preparation conditions. In true sol-gel processing routes, the reactivity of the reagents is high, and if alcohol exchange occurs or if modifying ligands are used, the structure of the species in solution can bear little resemblance to the starting compounds. In this case, the species that are generated are frequently oligomeric in nature and can contain more than one type of cation (Schwartz, 1997).

3.3 Nucleation and Growth of Particles in a Liquid Medium

The chemical reactions which transform a precursor solution, produce a large variety of complexes. The formation of solid particles from these complexes can be described as a process of nucleation and growth, according to the sequence;

$$\text{Hydrolyses} \Rightarrow \text{condensation} \Rightarrow \text{nucleation} \Rightarrow \text{growth} \qquad (3.13)$$

A succession of events of this type is not always the rule, chemical reactions can also proceeded so as to build at once a single monolith, by simultaneous merging of polymeric complexes results in polymeric gelation.

Solid particles can form as the results of heterogeneous on foreign inclusions, such as dusts, or the products from uncontrolled hydrolysis. The control of homogeneous nucleation rests on the successive steps illustrated in Figure 3.2, according to the model by La Mer. (Pierre, 1998). The growth rate (G) and the nucleation rate (N) are reported as a function of the concentration C in solute species. This solute can be any complex in the solution, resulting from hydrolysis and condensation of the precursors. The growth rate is non-zero above the solubility limit C_S, while nucleation requires a minimum supersaturation concentration $C_{min}^{nu} > C_S$ to occur (Figure 3.2).

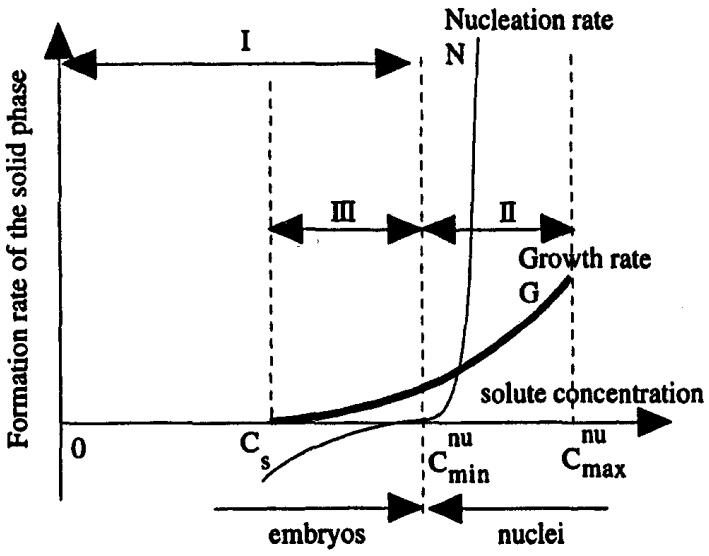

Figure 3.2 Variation of the nucleation and growth rates with the solid concentration (Pierre, 1998).

Nucleation occurs in region II, as well as growth. To stop nucleation, the solute concentration must be decreased below C_{min}^{nu} but maintained above C_S, so that only growth can keep proceeding (Figure 3.3).

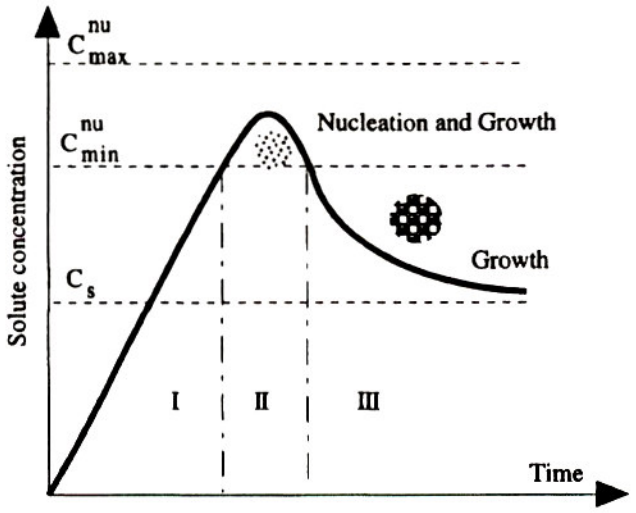

Figure 3.3 Simplified evolution of the solute concentration with time, during the homogeneous nucleation of particles. The domains I, II and III are the same as in the Figure 3.2 (Pierre, 1998).

3.4 Gelation

Gelation is a process according to which a sol, or a solution, transforms to a gel. It consists of establishing links between the sol particles or the solution molecules so as to form a 3-dimensional solid network.

Gelation occurs when the extent of polymerization reactions (ξ) reaches a critical value ξ_c. This precise critical stage, when for the first time a polymer of infinite size is formed, by comparison with the molecular scale, defines the Gel Point (GP). In a practical manner, at this point, the product resulting from polymeric condensations transforms suddenly from a viscous liquid to a material with elastic properties. In the liquid state a viscosity can be measured and its value increases towards infinity when coming near the gel point. In this model of gelation, called the Flory-Stockmayer model (or FS model), the infinite polymer is built by the successive addition of branches, all of which are constructed from the initial monomers (Pierre, 1998).

Gelation can be described in a more abstract fashion within the frame work of critical phenomena in thermodynamics in particular by the percolation theories. The

most simple of the percolation models are isotropic such as the bond percolation and the site percolation. In these models, either a bond is established or a site is occupied with connectedness probability p, in a completely random fashion throughout a geometrical network, as illustrated in Figure 3.4 on a planar square network.

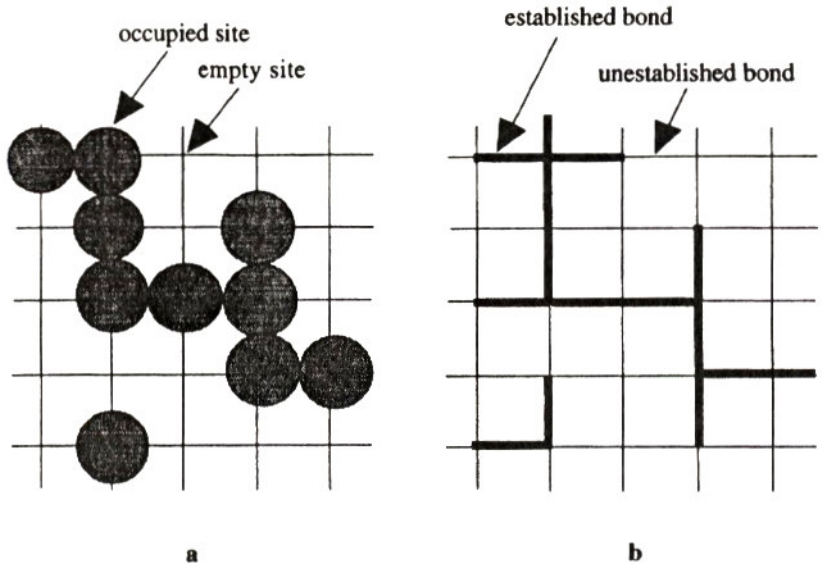

Figure 3.4 (a) Site percolation and (b) bond percolation on a square bi-dimensional network (Pierre, 1998).

The percolation theories show first the existence of a critical probability p_c, termed the percolation threshold (proportion of established links), such that if $p>p_c$ an infinite continuous cluster of bonds or of sites exists. The threshold corresponds to the GP in the case of gelation.

However, P_c value depends either on the coordination number (or functionality) Z in the case of a regular site network, or on the volume fraction ϕ occupied by the sites if they are replaced by hard spheres in a random fashion. The FS is one of the simplest models; its critical probability p_c is related to the coordination number Z by:

$$P_c = \xi_c = \frac{1}{Z-1} \qquad (3.14)$$

Its main default is to neglect the formation of closed loops, contrary to what occurs in real gelation.

Figure 3.5 shows that a quasi-linear relationship exists between P_c and either Z or ϕ (Pierre, 1998).

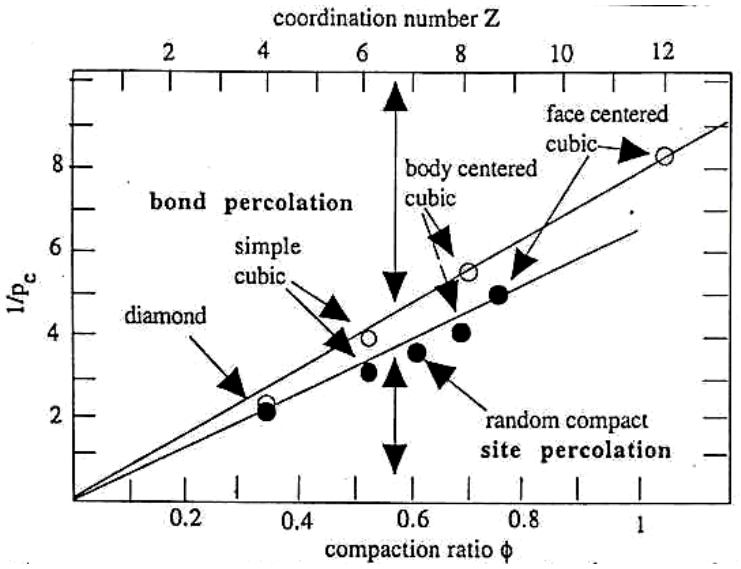

Figure 3.5-Empritical correlation between the percolation threshold and the lattice coordination for various three-dimensional structures (Pierre, 1998).

On the other hand, diffusion limited aggregation models (DLA model) show that fractal aggregates can also be formed by kinetic. In terms of this theory, the sites at a given distance from the original nucleus are allowed to walk randomly. They may therefore either avoid meeting a nucleus, or reach one of them and participate to its growth. As soon as some branches of the aggregate statistically start to grow around this nucleus, the possibility for sites to diffuse up the corridors without hitting a side branch becomes low. These branches have therefore a tendency to keep growing so that the aggregates becomes even more ramified than in the percolation models. The fractal dimensions of bidimensional models are 1.67 for DLA and 1.89 for percolation. The characteristics of the corresponding aggregates are illustrated in Figure 3.6. A refinement of DLA model considers several nucleation centers. Each nucleus grows by diffusion and simultaneously diffuses slowly. Hence, primary fractal DLA aggregates grow and finally aggregate themselves in a more open structure (Pierre, 1998).

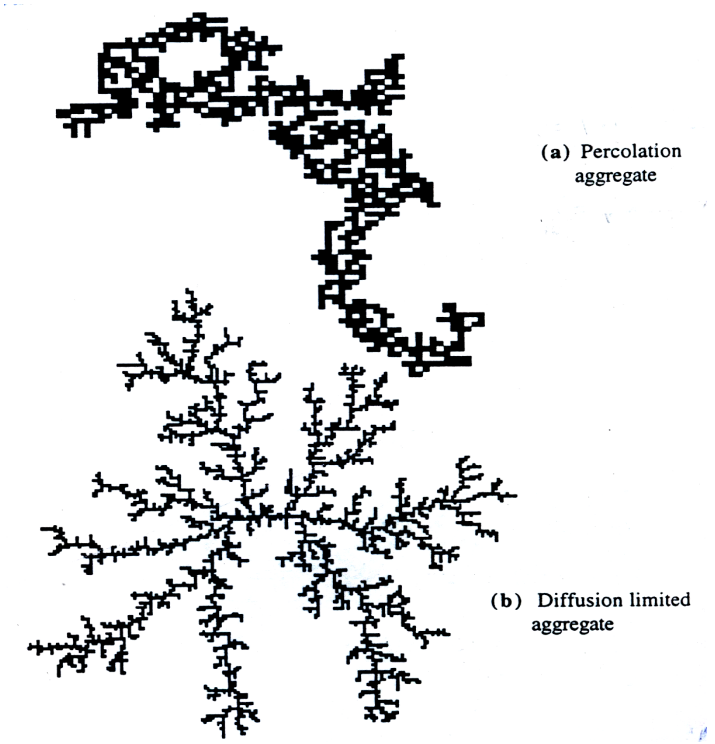

Figure 3.6 Bi-dimensional aggregates on a square lattice with different fractal dimensions: (a) aggregate near the percolation threshold in site percolation and (b) diffusion-limited aggregation cluster comprising 3600 particles (Pierre, 1998).

If the concentration C of non-potential determining electrolyte is smaller than the existence of a critical concentration for gelation C_g a sol is stable. If $C_c > C > C_g$, where C_c is the critical electrolyte concentration for coagulation, the sol slowly gels. If $C > C_c$, rapid coagulation occurs instead of gelation (Pierre, 1998).

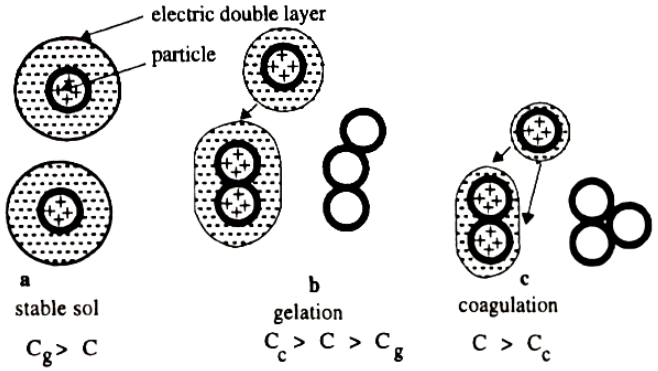

Figure 3.7 Conditions for the formation of: (a) stable sol; (b) gelation as a function of the non-potential determining electrolyte (Pierre, 1998).

3.5 Drying Gels

Drying rate per unit area of gels follows two successive regimes: a constant-rate period, followed by a falling-rate period (Figure 3.8, curves a and b). The transition between these two regimes occurs at a very sharp point named the critical-point (Pierre, 1998).

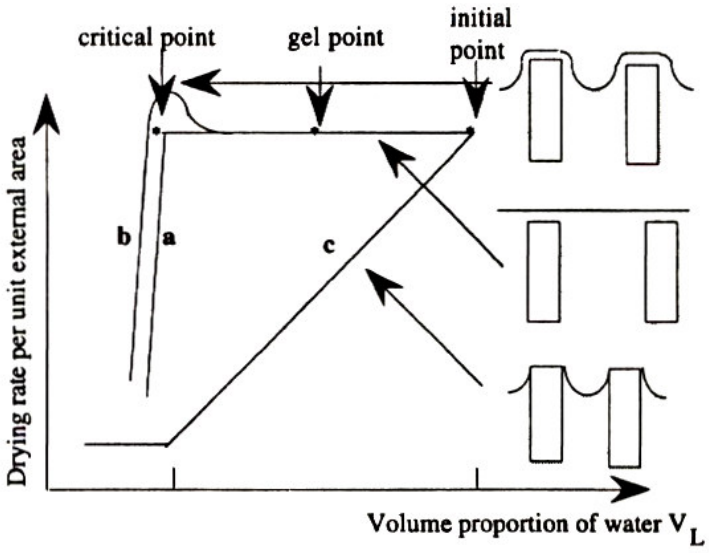

Figure 3.8 Evolution of the drying-rate per external unit area of wet gel as a function of the liquid volume proportion V_L: (a) and (b) experimental graphs; (c) graph if the drying rate was proportional to the relative surface of menisci (Pierre, 1998).

Drying is irreversible transformation of the gel which is composed of a solid network and liquid matrix. This capillary mechanism explains well the reproducible adsorption hysteresis curves of water in silica gels. This mechanism can be summarized as follows:

1) Evaporation creates a liquid vapor meniscus at the exit of pores in the gel.
2) This induces a hydrostatic tension in the liquid, which is balanced by an axial compression on the solid.
3) The latter compression makes the gel shrink.
4) As a result of shrinkage, more liquid is fed to the menisci at the exit of the gel pores, where it is evaporated and so on.

Branch IC in Figure 3.9a corresponds to the initial drying of the silica gel. C point is meniscus as in Figure 3.9b. Further on, it penetrates inside the gel pores which stop shrinking. Along CD, the meniscus is deeper inside the pores (Figure 3.9c), but this is a spherical meniscus with two radii of curvature equal to the radius of the pore r_{por}. Its curvature is therefore $2/r_{por}$. From D to S, only a thin layer of water remains on the cylindrical walls of the pores. The cylindrical configuration of point S maintains if water is readsorbed in the gel and the curve SDF is followed during re-adsorption. At point F, the gel pores are again full of water .Along FC, during the second desorption cycle, a spherical meniscus is formed again (Pierre, 1998).

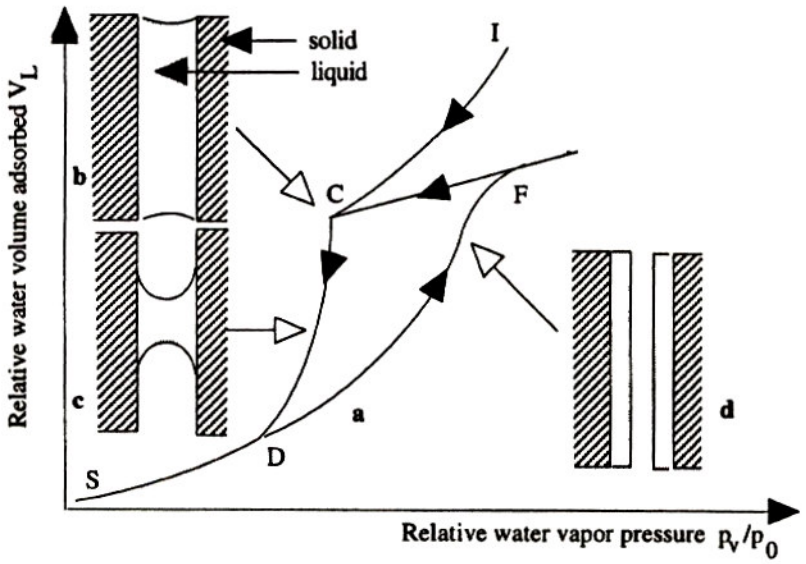

Figure 3. 9 Adsorption-desorption isotherms of water vapor in a silica gel (Pierre, 1998).

The equilibrium meniscus radius r_m at any instant is given by the compressive stress that the solid network of the gel can support. The contact wetting angle at the liquid–solid-vapor interface is undetermined along a sharp solid edge. Higher stresses are required for higher compression states of the solid, which requires higher hydrostatic tension in the liquid. It follows therefore that the menisci are sharper and sharper (smaller radius r_m) when contraction increases. This keeps a gel shrinking until the meniscus radius r_m reaches the pores radius r_{por}. The latter event defines the drying critical-point. Beyond this critical-point, capillarity cannot increase the compressive stresses anymore on the solid network. For instance, for a cylindrical pore of radius r_{por} and cross section.

Hence the drying rate per unit area should decrease linearly with the liquid content V_L (Figure 3.8 curve c). The experimental existence of a constant-rate period before the critical-point is therefore generally interpreted as being due to evaporation of a continuous liquid film, which covers the entire surface of the gel. Obviously the existence of such a film can be related to the affinity of oxides for water, which depends largely on the nature of the oxide (Pierre, 1998).

3.6 Phase Transformations During Heat Treatment

Once a gel is dried, it is often heated at temperatures much higher than for drying, so that transformation to more stable phases can occur. In many cases, this first involves a chemical evolution, each time a gel does not have the same chemical composition as the desired technical ceramic. Simultaneously, the matter composing the solid network undertakes a crystallographic reorganization and the pore texture changes. Such transformations proceed along kinetic routs which do not usually produce the most stable thermodynamic phases, but metastable ones, during the first steps. In a temperature range from 100 ^{o}C to 1000 ^{o}C which is termed intermediate temperature range, thermal treatments often produce either a crystalline transition phase or a glassy phase. These metastable phases eventually transform to a stable thermodynamic phases at high temperatures above 1000 ^{o}C by nucleation and growth (Pierre, 1998).

In this step, we have;

1. Removal of solvent or water (100 ^{o}C – 150 ^{o}C)
2. Combustion of carbon in the gel (250 ^{o}C – 350 ^{o}C)
3. Crystallization or oxidation (400 ^{o}C – 550 ^{o}C)

3.6.1 Chemical Transformations

In a temperature range which depends on gel being considered, but which typically goes from 100 ^{o}C to 300 ^{o}C, the crystallographic structure of the solid network remains close to what it was in the dry gel state. During this first stage, the

main transformation of a gel actually consists in a mass loss. One of the biggest contributions to the mass loss comes from the departure of the residual water. The latter can be divided in adsorbed water and structural water, also called ‘chemical water’ (Pierre, 1998). These two types of endothermic dehydration reactions occur at temperatures which largely depend on the synthesis conditions of a gel. If dehydration of adsorbed water is not properly occurred, the porous texture begins to change and in particular some pores can close and prevent the adsorbed water vapor to escape. To obtain uncracked ceramic samples, it is necessary to eliminate first the water adsorbed on the micropores walls before these pores can close.

The desorption of the chemical species adsorbed onto the pore walls is not limited only to water, it also concerns all types of solvents.

Another important contribution to the chemical evolution of a gel during its transformation at intermediate temperatures, concerning the residual organic groups which come either from an organic solvent or from the precursors. These residual OR can either hydrolyze at intermediate temperatures and be spontaneously eliminated as organic molecules such as alcohol, or they can remain in the pores of the gel network. In the latter case, they can be decomposed inside a gel and leave a carbon residue which gives a black color to the material. The decomposition of organics is a strongly exothermic reaction because of combustion of carbon. Exactly as with water, the decomposition of residual organics can be responsible for the formation of micropores.

The kinetic transformations at intermediate temperatures do not only consist in the formation of micropores by chemical decomposition. Some concurrent phenomena tend to reduce these micropores. One of these phenomena consists in a relaxation of the polymeric units which compose a gel network. This results in a continuous shrinkage of the solid material and permits more residual OH to come in contact with each other and to establish new metaloxane M-O-M bonds by condensation reactions. The network is therefore reinforced and densification begins according to a

process related to viscous flow, from which it differs by the important role played by the chemical reactions (Schwartz, 1997).

Chemical condensation reactions between residual OH groups are important preliminary steps in the evaluation of a gel towards a glassy or a crystalline phase. In the first step, they are responsible for a consolidation of the gel network with new active bonds forming.

The structure of a gel can also slowly transform by dissolution-recrystallization, in aqueous medium coming from its own dehydration water, adsorbed as well as chemical. Actually, heating a gel in the water coming from its own chemical water favors a faster crystallization.

Overall, the specific surface area of sol-gel materials decreases during heat treatment at intermediate temperatures. In the lowest temperature range, which depends on the material, this decrease is usually moderate and it accelerates as the temperature increases. Simultaneously, the grain size only grows moderately, so that the crystalline topology of the gel is roughly maintained. The new phases which are appearing are formed by transformations known as topotactic transformations (Pierre, 1998).

3.6.2 Topotactic Crystallization

At intermediate temperatures, that is to say in a temperature range which depends on the material but which does not exceed 1000 ^{o}C, the formation of new phases does not always occur by nucleation and growth, for kinetics reasons. This particularly true for the most stable thermodynamic phase, when nucleation requires a motion of both the cations and anions. This impossibility is due to the big size of anions such as oxygen anions which require high activation energy to move. Such an energy of thermal nature is not available because the temperatures too low. New crystalline phases can still form, but they do so in maintaining the some relative crystallographic positions of the anions as in the initial phase, namely in the initial

gel when a material is synthesized by sol-gel process. Such phenomena are not limited to gels however; they are quite common for the transformation at intermediate temperatures of all low temperature stable or metastable phases, such as the hydroxides.

Because they do not affect the relative near neighbor packing of anions, these transformations are named “topotactic transformations” (Pierre, 1998). Roughly, they keep the initial crystalline organization of the initial phase in terms of grains; a monocrystal remains a monocrystal.

In many cases, the new phases forming by topotactic transformation are not the most stable thermodynamic phases. They must be more stable than the initial phase, at a given temperature, but they can be metastable. This explains that a succession of topotactic transformations can be observed as the temperature is raised. More stable phases progressively appear, until the most stable thermodynamic phase is definitely formed. The intermediate phases are termed “transition phases” (Pierre, 1998). Of course, the sequences of topotactic transformations and intermediate phases formed depend on the initial gel structure, hence on the chemical recipe used in sol-gel processing. Topotactic transformations provide an explanation why different studies on a same compound lead to the production of different crystalline phases.

3.6.3 Crystallization by Nucleation and Growth

When gels are heat treated at increasing temperatures, the crystallization path sooner or later converges towards the most stable thermodynamic state. The stable diagram is reached at a temperature which depends on the type of ceramic and sol-gel process selected. In the cases where the stable crystalline phase first appears at a relatively low temperature, the formation mechanism is not always well established; it can very well be a topotactic transformation (Pierre, 1998).

To control the properties of the final ceramic film, an understanding of the thermodynamics and kinetics of the processes that take place during conversion of the solution precursor to the crystalline ceramic is required.

During crystallization, these solution precursor species rearrange to form an amorphous pyrolyzed film, which then transforms to the ceramic, by a nucleation and growth process. The characteristics of the nucleation-and-growth process will serve to define the resulting microstructure; films that display microstructures where only interface nucleation takes place are frequently columnar in nature, while those where nucleation occurs throughout the film are typically polycrystalline with equiaxed grains. From a thermodynamic perspective, it has been demonstrated that the driving forces that govern the transformation from the amorphous (pyrolyzed) film to the crystalline ceramic can play a significant role in defining the active nucleation events and, thereby, film microstructure, since it influences the barriers for nucleation of the crystalline phase at different locations (substrate interface, surface, bulk) within the film. A comparison of the thermal energy available (via heat treatment during the crystallization anneal) to overcome these different nucleation barriers will define which nucleation events take place and, thus, the resulting film microstructure. From standard nucleation and growth theory, the energy barriers for homogeneous and heterogeneous nucleation, and their dependence on driving force, are described by;

$$\Delta G^*_{\text{homo}} = 16\pi\gamma^3/3(\Delta G_v)^2 \tag{3.15}$$

$$\Delta G^*_{\text{hetero}} = \frac{16\pi\gamma^3}{3(\Delta G_v)^2} f(\theta) \tag{3.16}$$

where γ is the interfacial energy between the amorphous and the crystalline phase, ΔGv is the driving force for crystallization, i.e., the free energy difference per unit volume for the amorphous film-crystalline film transformation, and $f(\theta)$ is a function related to the contact angle, θ, according to equation 3.17 (Schwartz, 1997).

For a hemispherical nucleus on a planar substrate:

$$f(\theta) = (2 - 3\cos\theta + \cos^3\theta)/4 \qquad (3.17)$$

At the substrate surface amorphous phase has a higher interfacial energy than crystalline phase. When the nucleus forms on substrate, some high-energy substrate/amorphous surfaces are replaced by lower-energy substrate/nucleus surface. This contributes to a smaller overall interfacial energy in equation 3.18, resulting in reduction of the free energy barrier. Thus, the heterogeneous nucleation at the substrate surface is more likely to occur.

The θ value is determined by the surface energy of the substrate (γ_s) and the nucleus (γ_n) and the interfacial energy between them (γ_{sn}):

$$\cos\theta = \frac{\gamma_s - \gamma_{sn}}{\gamma_{sn}} \qquad (3.18)$$

Figure 3.10 shows a relationship between f(θ) and θ. The f(θ) value is increasing with the contact angle θ. Therefore ΔG^*_{hetero} in equation 3.16 is lower with smaller contact angle of the nucleus. $\gamma_{s=}\gamma_n$ and $\gamma_s=0$ in homoepitaxial systems give cosθ=1, f(θ)=0, and accordingly $\Delta G^*_{hetero}=0$. On the other extreme, $\gamma_{sn}=\gamma_s+\gamma_n$ gives $\Delta G^*_{hetero} = \Delta G^*_{homo}$, where the homogeneous nucleation occurs without the effect of the substrate.

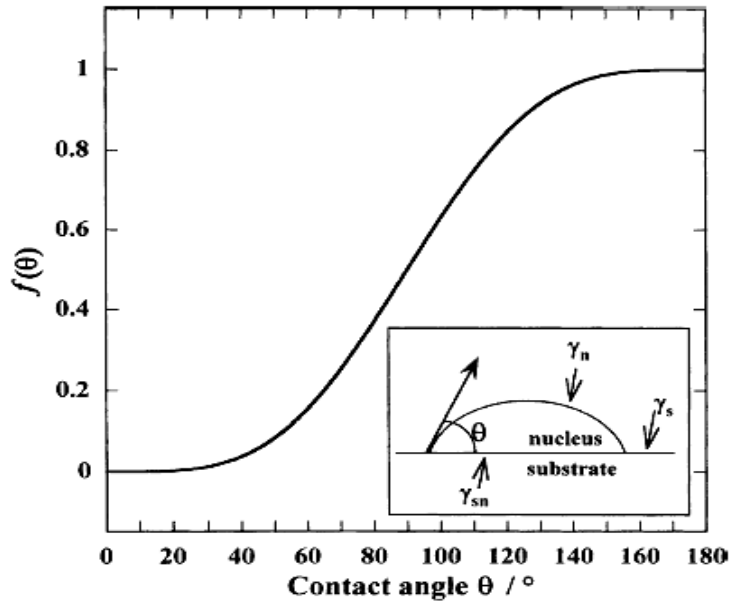

Figure 3.10 A relationship between f(θ) and contact angle θ (Pierre, 1998).

The difference in barrier heights for nucleation events such as interface, surface and bulk nucleation is therefore defined by the surface energy term, the driving force for crystallization, and the contact angle with the substrate.

Although more detailed analyses are possible, only a few concepts need to be kept in mind to understand film crystallization behavior: (1) As the crystallization driving force is increased, bulk nucleation becomes (essentially) as probable as interface nucleation. Although the f(θ) term still results in a lower energy barrier for interface nucleation, when crystallization driving force is high, i.e., in typical heat treatment situations, there is more than sufficient energy to overcome the energy barriers for all (including less energetically favorable) nucleation events. (2) The effects of crystallization temperature on driving force and nucleation must also be considered: crystallization at higher temperatures results in lower driving forces, and due to the f(θ) term, lower energy heterogeneous nucleation events become more important. (3)Unless rapid thermal processing techniques are used, film crystallization usually begins during heating to the anneal temperature. Therefore, as the temperature of the sample increases, more energy becomes available to overcome the barriers for nucleation events in addition to the energetically most favorable nucleation event. This can lead to film microstructures defined by nucleation and growth processes associated with more than one nucleation event. (4) The transformation pathway (from the amorphous film to the final crystalline ceramic) has a major effect on nucleation and growth behavior. Speck and co-workers have shown that for perovskite materials that transform via an intermediate metastable phase, e.g., PZT via a fluorite phase, the crystallization driving force is reduced by the formation of this metastable phase, this reduction in driving force separates the energy barrier heights for different nucleation events and makes interface nucleation in PZT much more preferred than bulk nucleation, resulting in films that display only heterogeneous nucleation at the substrate interface. To fully consider thermodynamic driving force effects, we need to know the free energies of the amorphous states, the free energies of the crystalline states, the crystallization temperatures, and the transformation pathways. The use of substrates with a higher level of lattice matching and of the same crystallographic structure as the perovskite film would be

expected to decrease the value of f(θ). This would lower the energy barrier for nucleation at the substrate interface compared to nucleation within the bulk of the film (Schwartz, 1997).

3.7 Sintering

Simultaneously with the transformations of a gel to ceramics, the specific surface area of sol-gel materials decreases during thermal treatments. The progressive elimination of the porosity is an evolution named sintering. In terms of thermodynamics, sintering originates from the specific surface area S_a of a porous material, which introduce a positive contribution G_s due to the surface of pores, to the Gibbs free energy of a material (Pierre, 1998):

$$G_s = \gamma S_a \tag{3.19}$$

Since states with a lower Gibbs free energy are more stable at a given temperature and pressure, the specific surface area should tend to decrease, an evaluation which can proceed according to two types of pore evolution:

1) by changing the shape of pores but not their volume.
2) by eliminating the pores.

The first type of evaluation does not produce any material densification, contrary to the second one which makes a material shrink without losing any mass. Moreover, sintering is not the only transformation which involves Gibbs free energy of surface origin. Grain boundaries constitute another type of surfaces which contribute another Gibbs free energy term G_{gb}. In order to reduce this free energy contribution, the specific grain boundary area S_{gb} must decrease. Hence another evolution named grain growth enters in competition with sintering (Pierre, 1998).

Sol-gel ceramics just after drying and even after heat treatments at intermediate temperatures often have a very high specific surface area and an extremely small

grain size. Hence, both sintering and grain growth tend to be vigorous (Schwartz, 1997).

3.7.1 Thermodynamics and Kinetics of Possible Texture Evolution

Inside a solid particle, near an external surface such as a pore surface, mechanical stresses are introduced by the surface tension each time the surface is curved. If the external pressure in the pores outside the solid is p_o and the two principal curvature radii of the surface are r_1 and r_2, the local pressure inside the solid, just under the surface is (Pierre, 1998).

$$p = p_o + \gamma\left(\frac{1}{r_1} + \frac{1}{r_2}\right) \tag{3.20}$$

When the local surface is convex, that is to say when the solid is on the same side as the center of curvature, a radius r must be taken with a positive value. On the other hand, when the local surface is concave, that is to say when the solid is on the opposite side to the center of curvature, the radius r must be taken with a negative sign. For sake of simplicity, it is possible to consider the case where $p_o=0$ (treatment under vacuum). In such conditions, when two spherical particles of radius r are linked by a neck with principal radii x (convex radius) and p (concave radius) at the neck tip and such that in absolute value $p<<x$, (Figure 3.11), the mechanical stresses states inside the solid near the external surface are:

- a compression far from the neck, at point A where:

$$p_A = \sigma_c = \frac{2\gamma}{r} > 0 \tag{3.21}$$

- a tension near the neck at point N where:

$$p_N = \sigma_t = \gamma\left(\frac{1}{x} - \frac{1}{\rho}\right) \approx -\gamma\frac{1}{\rho} < 0 \tag{3.22}$$

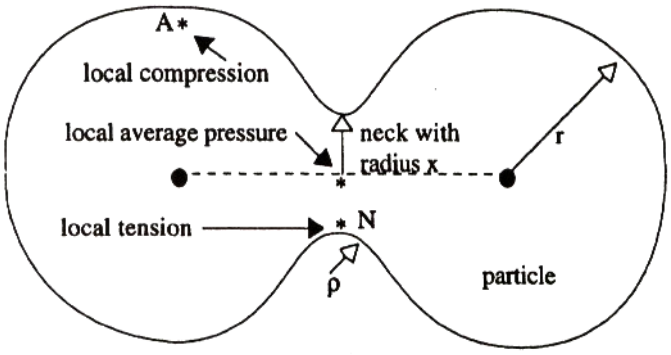

Figure 3.11 Initial sintering stage of two spherical particles (Pierre, 1998).

This mechanical stress difference between points A and N is equivalent to a difference in the local Gibbs free energy of mechanical nature and it tends to attenuate by transfer of matter. Finally, the surface energy happens to be at the origin of atomic transport.

In terms of kinetics, the transport of atoms to sinter a material can proceed along several different types of paths. Some of these paths actually result in densification, in particular when the atoms originate from sources, that is to say local parts of the material located along dislocations and grain boundaries, or when atoms are transported by a cooperative phenomenon known as viscous flow. Other transport paths only change the pore shape, in particular when the matter comes from the pore surface (Pierre, 1998).

3.7.2 Atomic Transport Mechanisms Operating During Sintering

When sintering proceeds by atomic diffusion in the case of a ceramic which comprises several types of ions, each ion has to diffuse in proportion to its stoichiometry in the ceramic. Consequently, sintering is controlled by the slowest ion transported along its fastest path. If one species, for instance the anions, has the smallest diffusion coefficient, it is possible to accelerate its diffusion with the help of cations additives which have a lower valence and a size close to that of the host cation. To balance the electric charges in the compound, anion vacancies are then often created, which accelerates anions diffusion. In oxide, this concerns the oxygen

anions which diffuse significantly at high temperature only. The formation of oxygen vacancies increases their mobility and can help sintering. The proportion of additives must remain below but can be close to the solid solution limit (Pierre, 1998).

3.7.2.1 Atomic Diffusion in Sol-Gel Materials

It is possible to question whether transport mechanisms such as atomic diffusion can be extrapolated from the conventional ceramics, to the colloidal sizes. Atomic transport by diffusion in the vapor phase rests on an evaporation-condensation process due to differences in the equilibrium vapor pressure near a solid surface, depending on the local surface curvature. The equilibrium vapor pressure is lower near a neck between two particles where the solid surface is essentially concave, than far from a neck, at atomic scales. The resulting vapor pressure gradient induces a vapor phase diffusion which keeps feeding the neck. It modifies the pore shape but does not induce densification which in a gel often occurs between 900 and 1200 ^{o}C. At these temperatures, the equilibrium vapor pressure of oxygen is very low for an oxide. On the other hand, the residual hydration water usually absent in conventional ceramics is much more volatile relatively low temperatures. Hence, this mechanism cannot be completely rejected for the sol-gel processes, as water is known to be a general sintering aid (Pierre, 1998).

Surface atomic diffusion does not induce densification neither. However, it is like to operate at a lower temperature than usual, because of the extremely high special area of sol-gel and also because of the special nature of the gel surface which easily adsorbs water molecules or OH groups (Pierre, 1998).

Overall, the atomic transport mechanisms which make the pore shape become spherical without producing any densification are likely to be common in sol-gel materials. If this is the case, these mechanisms can be strongly modified by tailoring the nature of a sol-gel solid surface, for instance by adsorbing hydrophobic molecules. Hence the liquid sol-gel chemistry can have a marked influence on the sintering behavior (Pierre, 1998).

Lattice atomic diffusion can actually densify a material, depending on the source from where the atoms originate. In a crystalline material such as an oxide, this mechanism begins to significantly operate when the atomic mobility of oxygen atoms is high enough that is to say at high temperatures. It requires the presence of atomic point defects such as vacancies, interstitialcies, or dislocations. However gels are far from being very well crystallized; they have at best very small grains whit a high defects density. Consequently, depending on the compound, lattice diffusion can often operate at a much lower temperature than conventional ceramics. Actually, a distinction between the different atomic diffusion paths, such as on a surface, inside a lattice, along dislocations or along grain boundaries may be difficult in sol-gel materials, in so far as it becomes difficult distinguish between dislocations, grain boundaries and surfaces (Pierre, 1998).

3.7.2.2 Sintering and Crystallization in Sol-Gel Ceramics

In so far as densification can be considered to occur in sol-gel ceramics by global atomic diffusion, the corresponding diffusing species are also likely to enhance the crystallization by nucleation and growth of the most thermodynamically stable crystalline phase. Densification of sol-gel ceramics often occur concurrently with their crystallization. Even in compounds where sintering occurs at a relatively low temperature, the crystallization of a stable phase usually occurs at a slightly lower but very close temperature (Pierre, 1998).

All the hydrolysis-condensation conditions of sol-gel synthesis have an effect on the sintering rate, in the same way as they are responsible for a large variability in the nature of the first phases which crystallize.

3.3.4 Advantages and Limitations of Sol-Gel Processing

There are many advantages to sol-gel processing. It not only allows for materials to have any oxide composition, but it also permits the production of new hybrid

organic-inorganic materials which do not exist naturally. Sol-gel processing also has many other significant advantages. Very pure products are obtained by simply purifying the precursors either by distillation, crystallization, or electrolysis. Moreover, the chemical processes of the first steps are always carried out at low temperatures. By comparison with the classical high temperature synthesis of conventional ceramics, this minimizes considerably the chemical interactions between the material and the container walls. Another advantage is the association of the solid colloidal state with a liquid medium, thus avoiding any pollution by the eventual dispersion of dust. This explains why the biggest industrial application of sol-gel synthesis of ceramics is for nuclear fuels; pollution is very critical in this domain.

There are other more fundamental advantages to sol-gel processing. For instance, the kinetics of the various chemical reactions can be easily controlled by the low processing temperatures and by the often dilute conditions. The nucleation and growth of the primary colloidal particles can also be controlled in order to give particles with a given shape, size, and size distribution.

Sol-gel processing offers the most outstanding advantages for mixed oxides systems in which the chemical homogeneity of the various elements can be controlled down to the atomic level. This is case of the Lead Lanthanum Zirconium Titanates solid powders are mechanically mixed such as in the conventional processes; and hence the optical transparencies obtained are, in this case, not as high as those obtained by sol-gel processing (Pierre, 1998).

The greatest limitation to the synthesis of ceramic by sol-gel processing is still the cost of the precursors, and especially that of alkoxides. Most of these alkoxides are however quite easy to make; especially if they do not tend to polymerize. A few of them such as Zr and Ti (Pierre, 1998). Moreover, alkoxides can also be mixed with much cheaper metal salts provided that a purification step is included in the procedure.

CHAPTER 4
EXPERIMENTAL STUDIES

4.1 Purpose

The sol-gel technique for preparation of ferroelectric thin films has many advantages such as easier composition control, better homogeneity, non-vacuum process, lower processing temperature, lower cost, and easier fabrication of large area films (Bao at al., 2002).

In recent years, there has attracted considerable attention on using sol-gel process to prepare ceramics from metal alkoxides, because high-purity, ultrafine particles and large-area films can be prepared at relatively low temperature (Zeng at al., 2002).

The objective of this study was to synthesis and characterization of $PbTiO_3$ thin films by a sol-gel technique from their metal alkoxides and measure dielectric properties of the films. The structure of the obtained thin films was characterized by x-ray diffractometer (XRD), the surface morphology of the thin films was examined using scanning electron microscope (SEM), elemental analyses of the films was observed with energy-dispersive x-ray spectroscopy (EDS), the mechanism of $PbTiO_3$ formation through dried gel to crystallite conversion were investigated by thermogravimetric analysis (TGA) and differential thermal analysis (DTA) and dielectric properties were measured using dielectric analyzer. These properties were determined for films were prepared with various processing parameters and were compared.

4.2 Materials

In the present work, two purified metal-organic precursors, namely titanium (IV) isopropoxide, $Ti[OCH(CH_3)_2]_4$ (>97%min.), and lead (II) acetate trihydrate, $Pb(CH_3COO)_2.3H_2O$ (>99.5%), were used to obtain $PbTiO_3$ (Pb: Ti=1:1) solutions. Ethylene glycol, $C_2H_6O_2$ (>99.5%), was used as a solvent to dissolve all compounds

to form solution. The optimal amount of glacial acetic acid, CH_3COOH (100%), was used as a catalyst and for modifying the solutions on a molecular level, which resultant in homogeneous solution.

4.3 Preparation of Thin Films

The $PbTiO_3$ film grown on commercially glass substrates by sol-gel process is shown schematically in Figure 4.1. Firstly, lead acetate was dissolved in glacial acetic acid and ethylene glycol in air atmosphere at room temperature, and then titanium (IV) isopropoxide was added drop wise to the mixture to yield 1:1 molar ratio of lead to titanium. Four different solutions are prepared by using different amount of ethylene glycol, namely 2 ml, 4 ml, 6 ml and 8 ml, to provide $PbTiO_3$ films with optimum characteristics. Solutions were mixed by a magnetic stirrer until a clear solution developed at room temperature for approximately 1 hour in air to ensure the formation of the homogeneous $PbTiO_3$ sol. Not only glasses were chosen as substrates but also stainless steel plates were used to observe electrical properties of these films. The precursor solutions were then deposited on the clean glass substrates by the dip-coating method to obtain the wet gel films, which were then dried at 300 ^{o}C for 5 min to evaporate water, alcohol and the organics (pyrolysis). The dip-coating and drying processes were repeated many times to get desired film thickness. In this step, the gel shrank and lost weight through the evaporation of solvent and adsorbed water. This is a critical step in the processing of the films because cracks and other defects are most likely to develop in this stage named at pyrolyzing the organics, leaving tiny pores throughout the film. These pores were later eliminated by an annealing mechanism by heating the films in a furnace at 600 °C for 1 hour in air. The whole process of the heat treatment is completed in air atmosphere. After the annealing, the samples were cooled spontaneously under fire condition.

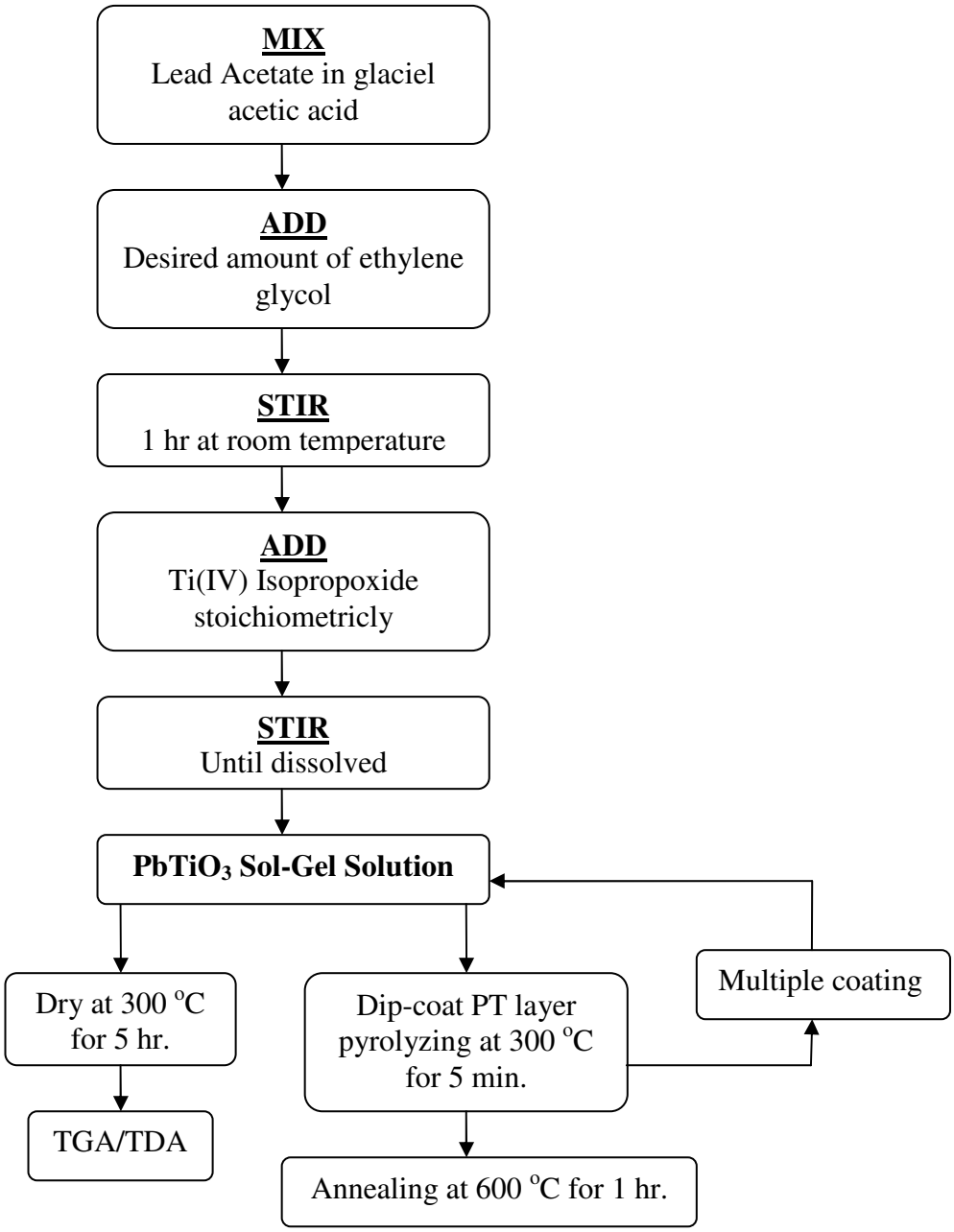

Figure 4.1 Flow chart of thin film deposition by using sol-gel method.

4.4 Characterization

4.4.1 pH Measurement of Solutions

The pH values of the solutions used were measured by a standard pH meter with Mettler Toledo electrode. It was observed that the solutions are acidic or basic character.

4.4.2 Differential Thermal and Thermogravimetric Analysis

Prior to DTA-TGA measurement, samples which were dried gel at 300 °C for 5 h in air were prepared from the solution. For TGA, sample is loaded onto an accurate balance and it is heated at a controlled rate, the results reveal the temperatures at which the mass of the sample changes. In DTA, sample and a reference material (Al_2O_3 for this work) are heated at a constant rate while their temperatures are carefully monitored. Whenever the sample undergoes a phase transition (including decomposition) the temperature of the sample and reference material will differ. If the phase transition is endothermic, the sample will be hotter than the reference material. If the phase transition is endothermic the sample will be cooler. DTA is useful for determining the presence and temperatures at which phase transitions occur, and whether or not a phase transition is exothermic or endothermic. DTA is often used in combination with TGA. DTA and TGA for the dried gel were performed in platinum crucibles, at heating rate 10 °C/min. up to 700 °C in air using a Shimadzu thermal analyzer DT-60H.

4.4.3 X-ray Diffraction (XRD)

X-ray diffraction is an ideal method for determining the crystalline phases of materials. Each material with crystalline structure forms unique characteristic diffraction pattern when exposed to radiation by X-ray source. This provided pattern from the unknown material is used to identify that material. The phase structure of the sol-gel coated $PbTiO_3$ thin films was determined by the X-ray diffraction (XRD) analysis instrument (Model: Rigaku , D/Max-2200/PC diffractometer) using Cu Kα radiation with a voltage and current of 40 KV, 20 Ma, respectively.

4.4.3 Scanning Electron Microscope (SEM)

In the SEM, a fast electron beam is focused into the specimen and interaction occurs between the electrons and atoms of the specimen, it creates various signals which can be collected by appropriate detectors.

Surface morphology and microstructure of the thin films were characterized by JEOL JSM-6060 type scanning electron microscope (SEM) using a secondary electron image (SEI) and the operation voltage was set to be 20 kV. Before SEM observations, the samples were coated with an Au-Pd to being conductive by Polaron Range Sputter Coater with a current of 10 mA for 90 second.

4.4.4 Energy-Dispersive X-ray Spectroscopy (EDS)

EDS is a technique of x-ray spectroscopy that is based on collection and energy dispersion of characteristic x-rays. Energy dispersive x-ray detectors can be used for element detection in the SEM. When the atoms in a material are ionized by high-energy electrons, they emit characteristic x-rays, which enter solid-state detector in an EDS spectrometer are converted into signals that can be processed by the electronics into an x-ray energy map in which the concentration distribution of an element of interest is displayed on a micrograph or an x-ray energy histogram. In this study, elemental analyses and x-ray map taken from point and regional analyses of the specimens surfaces were observed with a 500 Digital Processing (IXRF Systems, Inc.) model energy-dispersive x-ray spectroscopy (EDS).

4.4.5 Electrical Characterization

In order to use in electrical characterization of the thin films, the refractive index and the thickness of the films on the glass substrates were measured by an Abbe Refractometer and a JASCO V-530 UV/VIS spectrophotometer, respectively.

In order to conduct electrical measurement on the $PbTiO_3$ films, samples were also prepared on stainless steel substrates under the same processing conditions as previously mentioned. The dependence of the dielectric permittivity (ε') and loss tangent ($\tan\delta$) on the frequency were measured at room temperature using an Alpha-N High Resolution Dielectric Analyzer (Novacontrol Technologies).

In a dielectric or impedance measurement a voltage V_0 with a fixed frequency $\omega/2\pi$ (sinusoidal voltage) is generally applied to a sample cell which contains the sample material under test. V_0 causes a current I_0 at the same frequency in the sample cell. In addition, there will be a phase shift between current and voltage described by the phase angle φ which causes to form ε' (real dielectric constant) and ε'' (imaginary dielectric constant). Tan loss, defined as the ratio ε'' (imaginary dielectric constant) to ε' (real dielectric constant), can be obtained. The electromagnetic properties of the sample material and the sample geometry determine the ratio of I_0 and V_0 and the phase angle ϕ.

CHAPTER 5
RESULTS AND DISCUSSION

5.1 The pH Values of The Solutions

Figure 5.1 shows the change of pH values of the solutions as a function of the amount of the solvent (ethylene glycol). As seen from this curve, the solution becomes increasingly alkaline with increasing ethylene glycol. The pH is an important factor that affects the formation of network structure during gelation. Randomly branched structure is formed under the acidic conditions; separated clusters appear under the basic conditions.

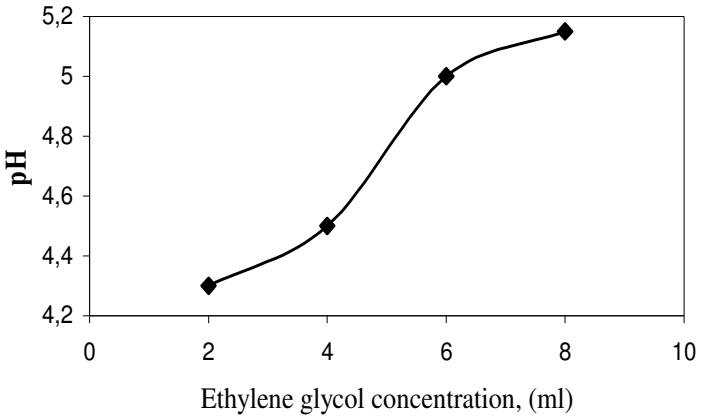

Figure 5.1 The pH values of the solutions versus the amount of ethylene glycol in the solution.

5.2 TGA and DTA Analyses

Figure 5.2 shows the DTA and TGA curves for the dried gel in powder form prepared by $PbTiO_3$ precursor solution. A large weight loss (3,953%) in TGA curve observed between 34,60 °C and 352,18 °C accompanied by exothermal peak in DTA curve around 340 °C is probably due to (i) the evaporation of residual solvent, (ii) the removal and decomposition of acetyl groups and bonded alkyl groups coming from solvent, chelating agent and precursors and their combustion. Regarding the DTA curve, a broad exothermal peak observed around 438 °C can be attributed to

formation of oxidative reactions forming PbO, TiO_2, Ti_3O_5 and $PbTiO_3$ complexes which were observed from XRD results. At least, a very weak exothermic peak at about 550 °C without mass loss can be attributed to the crystallization of the perovskite $PbTiO_3$ lattice. These results are in good agreement with Bao et al., 2002. As DTA and TGA results indicated, the thin films have to be heat treated at temperature of 600 °C.

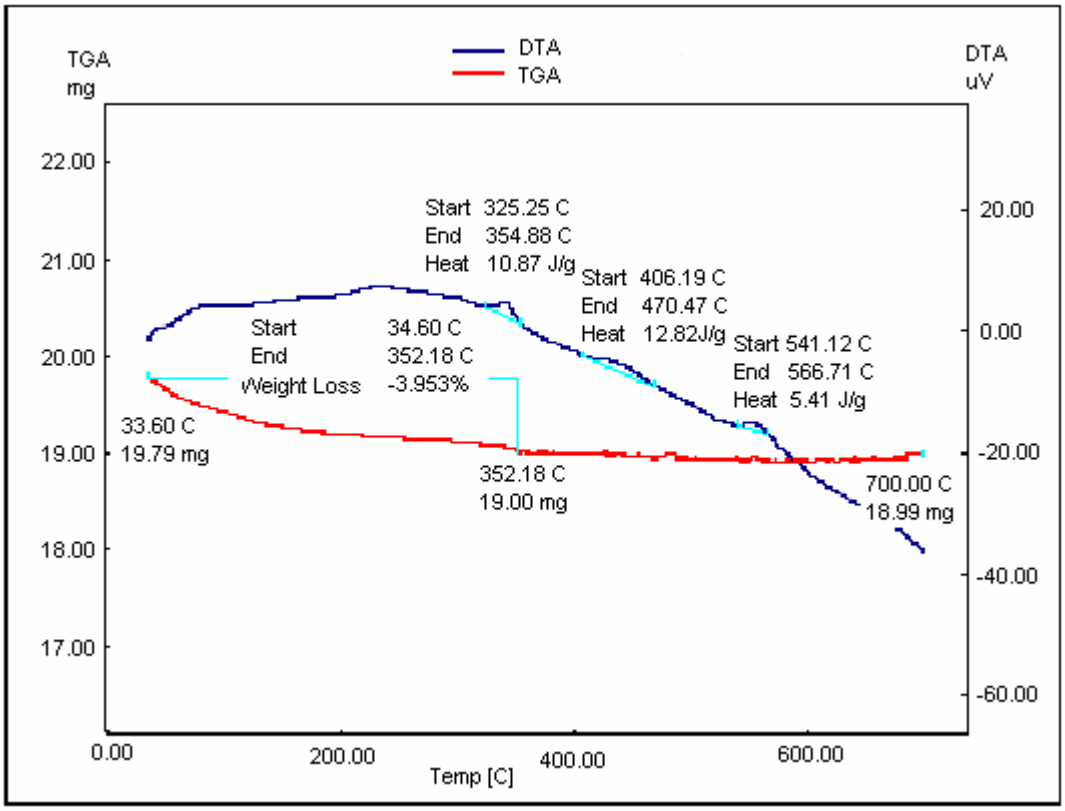

Figure 5.2 DTA – TGA curves for the dried $PbTiO_3$ gel.

5.3 Phase Analysis

The crystalline nature of the films was analyzed by XRD technique, and the effect of annealing temperature on film crystallinity was studied. After pre-annealing heat treatment at 300 ^oC, XRD indicated that the pyrolysed films were found to be amorphous, and post-deposition annealing was required to develop crystallinity (Lai et al, 1998). At 400 ^oC, peaks related to the perovskite structure of the $PbTiO_3$ phase (Macedonite) appeared. In this case, the $PbTiO_3$ did not crystallize well and

additionally intermediate metastable phases such as PbO, TiO_2 and Ti_3O_5 were found (Figure 5.3).

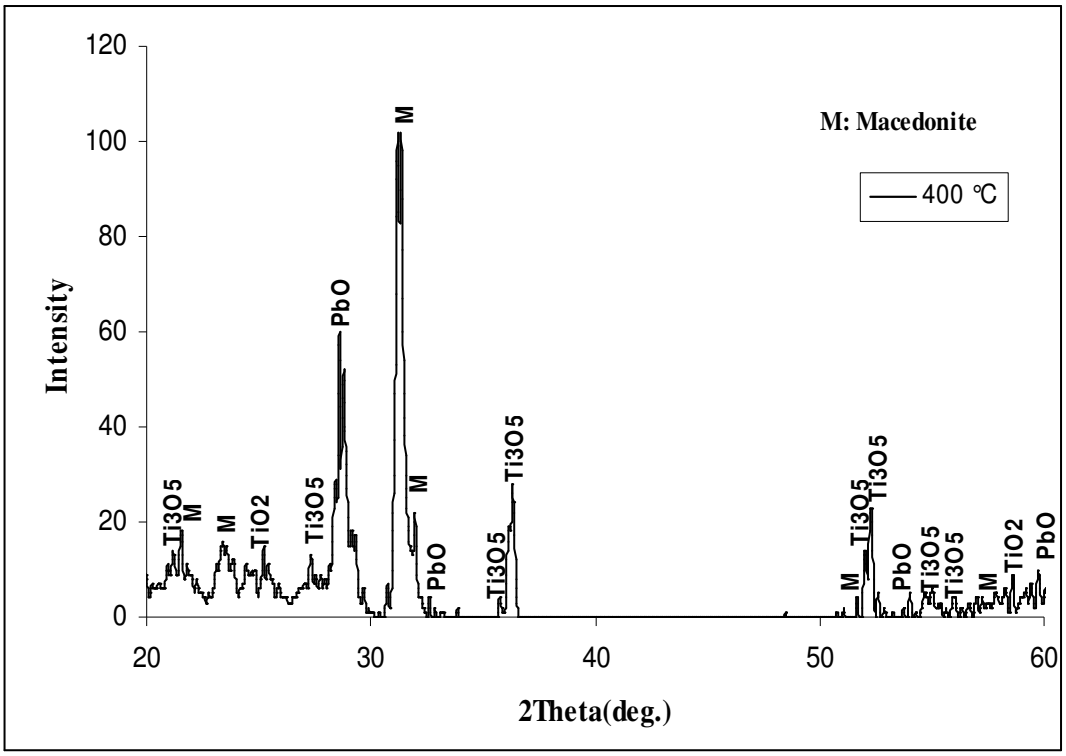

Figure 5.3 XRD pattern of the $PbTiO_3$ thin film on glass substrate annealed at 400 °C in air for 1 hr.

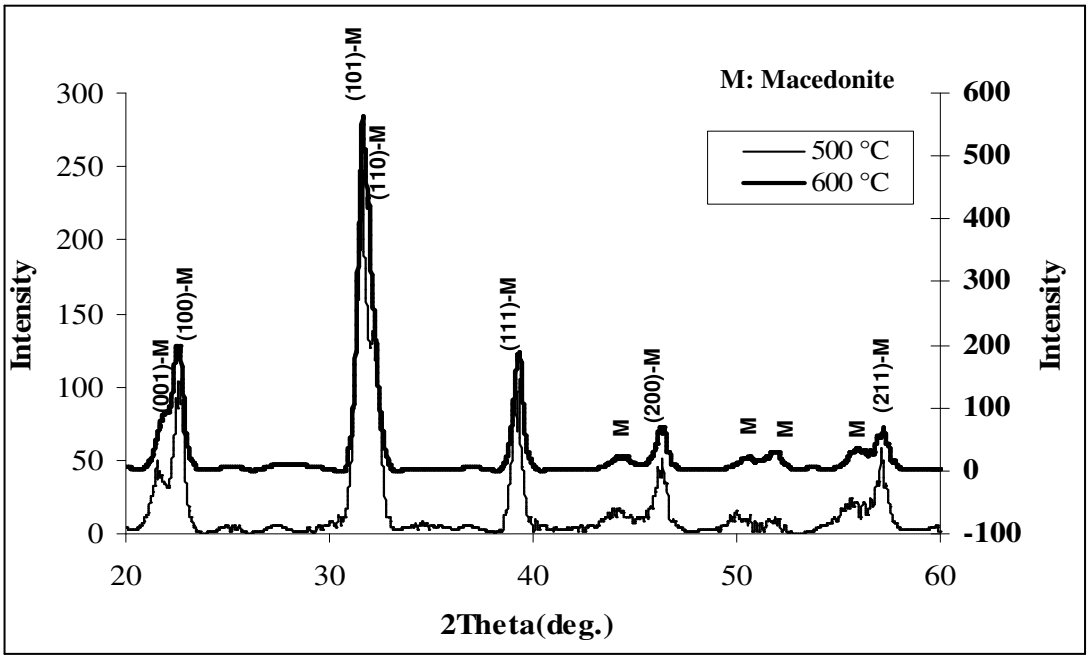

Figure 5.4 XRD patterns of the $PbTiO_3$ thin films on glass substrates annealed at 500 °C and 600 °C in air for 1 hr.

Figure 5.4 shows the X-ray diffraction spectra of films annealed at 500°C and 600 ^{o}C. Film annealed at 500 °C converted into a perovskite crystalline phase without intermediate phases compared to the thin film annealed at 400 ^{o}C. However, both thin films annealed at 500 and 600 °C have the perovskite structures but the peaks became sharper and more intense at 600 °C indicating better crystallinity and increased grain size. Well crystallized $PbTiO_3$ films were produced at an annealing temperature of 600 °C. This indicates that the thin film has crystallized to the $PbTiO_3$ single phase and the polycrystalline nature. All the peaks are characteristic of the tetragonal perovskite structure of the $PbTiO_3$ phase (Macedonite) corresponding to the (001), (100), (101), (110), (111), (200) and (211) orientations. Similar results can be found in reference (Cheng et al., 2000).

Also, it is clear that no peak indicating to the substrate was observed. A problem associated with the deposition of ferroelectric films on soda-lime glass is the out-diffusion of Na^{+} from the glass substrate to the film during heat treatment (Cheng et al. 2000). However, in the present study, no impurity phase could be found in the $PbTiO_3$ films suggesting a significant out-diffusion of the Na^{+}, Ca^{2+}, or Si^{4+} ions from the soda-lime glass into the film.

5.4 Microstructural Examination

Figure 5.5 shows the scanning electron micrographs of the surfaces of the $PbTiO_3$ thin films with different amount of solvent on glass substrates annealed at 600 °C for 1 h. Compared with Figure 5.5 it was found that the crack formation obviously decreased with increasing amount of solvent in solution. This result is because of lower viscosity of solutions with higher amount of solvent which cause a better spreading of solutions on substrates during heat treatment (see Figures 5.5a, and 5.5b). The homogeneous films with some cracks were obtained because of diluted solutions which contain a solvent of 6 ml as shown in Figure 5.5c. Therefore, it is indicated from the Figure 5.5 (d), it was observed that the best film surface was provided from the thin films with a solvent of 8 ml. in its solution.

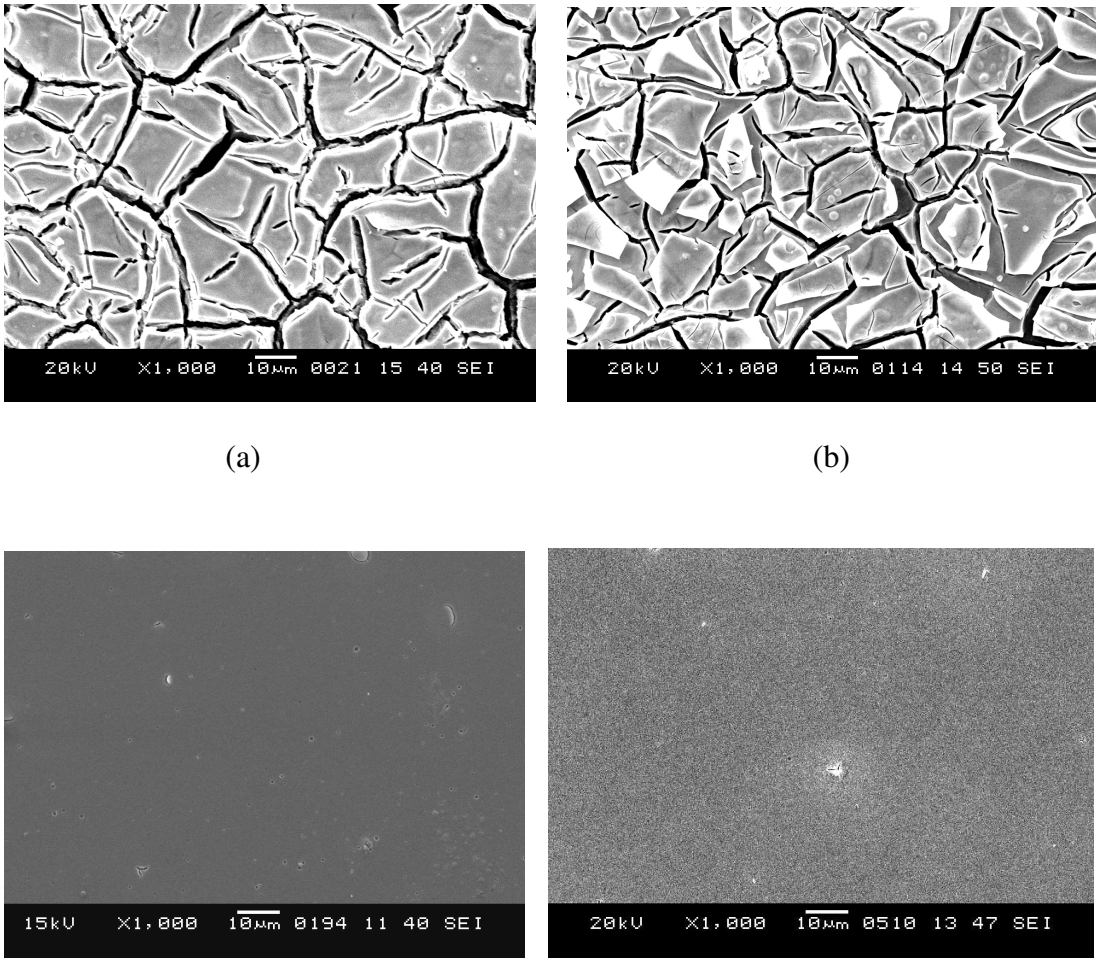

Figure 5.5 SEM images (magnification of 1.000X) of the surface morphology of $PbTiO_3$ thin films with different amount of solvents: (a) 2 ml., (b) 4 ml., (c) 6 ml. and (d) 8 ml.

The SEM images of the surface morphology of the films with different thickness are shown in Figure 5.6. The film with 4 layers displayed a dense, homogenous morphology with fine grains, with no obvious (Figure 5.6a). On the other hand, there are many large cracks appeared in the films with 6 layers, and 8 layers, as shown in Figure 5.6b, c. In the chemical solution decomposition method, the stresses due to the shrinkage of the green film during thermal treatment developed as the film thickness increased. When the thickness reaches a critical value, the huge stress in the film always leads to the film cracking, as demonstrated in (He et al., 2003).

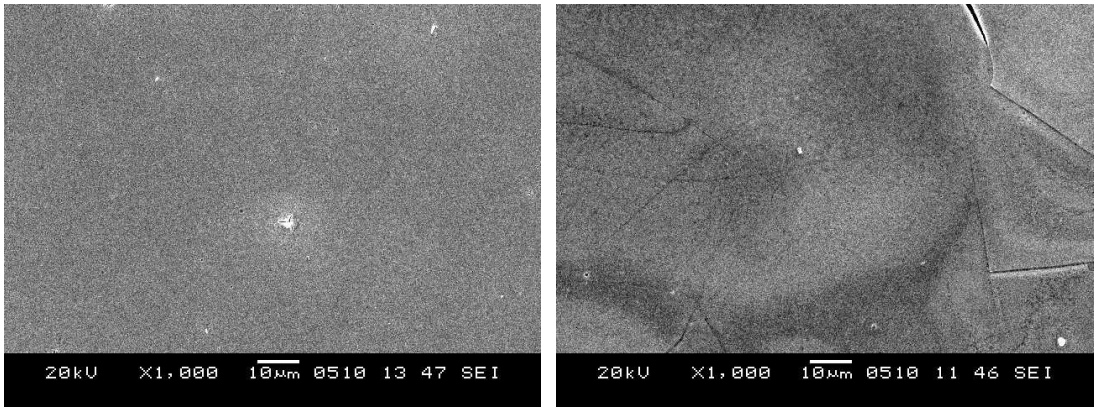

(a) (b)

(c)

Figure 5.6. SEM images (magnification of 1.000X) of the surface morphology of optimum $PbTiO_3$ thin films (from Figure 5.5.d) with different thickness (a) 3, (b) 6, and (c) 9 coating layers.

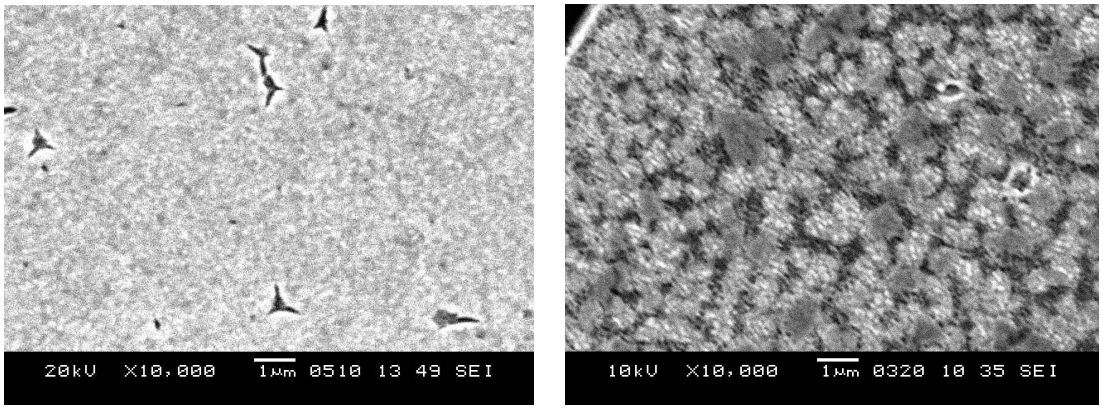

(a) (b)

Figure 5.7 SEM micrographs (magnification of 10.000X) of the $PbTiO_3$ thin films with (a) 3, (b) 9 coating layers.

The microstructure of the surfaces of the films with 3 coating layers and 9 coating layers are shown in Figure 5.7. Figure 5.7(a) shows a fine-grained, homogeneously distributed microstructure with micro-cracks, although Figure 5.7(b) showed a few particulate structures with a size of about 1 μm. Having considered that the film thickness is high, such surface fluctuation or roughness is understandable found elsewhere (Ma et al., 1995).

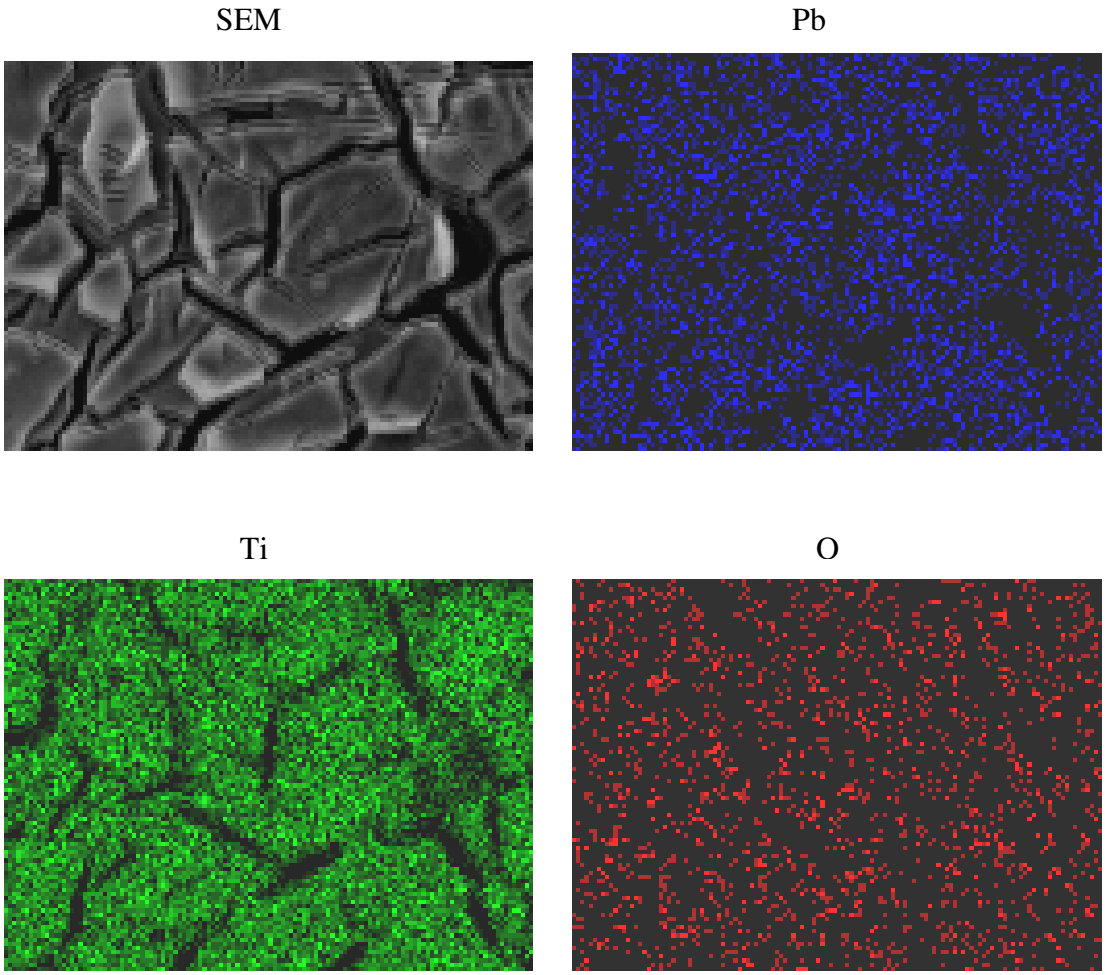

Figure 5.8 SEM micrograph and X-ray maps of the $PbTiO_3$ thin films with a solvent of 4 ml. in its solution.

Figure 5.8 shows SEM micrograph of the $PbTiO_3$ thin films and X-ray maps of Pb, Ti and O elements in the films. It is clear that Pb and Ti regularly distributed in the films. In addition to this, it was observed from the EDS analyses of the thin film at magnification of 10.000X, a percentage distribution of elements, such as Pb, Ti

and O, in the film corresponded to the stoichiometry of the $PbTiO_3$ phase. This also supported that perovskite structure formed in thin film structure (see Figure 5.9).

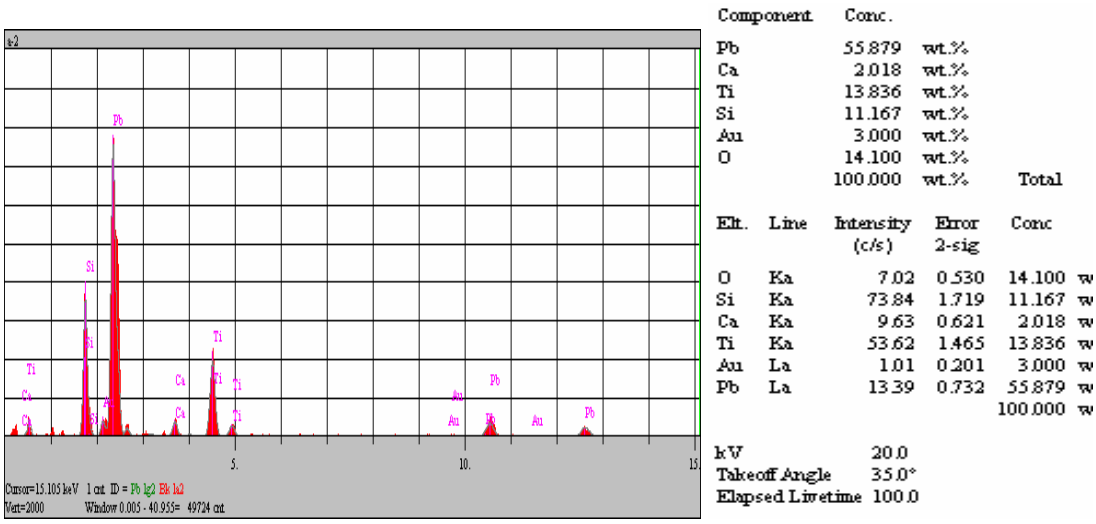

Figure 5.9 EDS analysis of the $PbTiO_3$ thin film at magnification of 10.000X.

5.5 Electrical Properties

The dielectric constant (ε′) and dielectric loss (tanδ) measurements were performed at room temperature as a function of frequency in the range of 10^{-2}–10^{6} Hz for the coated thin films with different thickness on stainless steel substrates. The total $PbTiO_3$ thickness reached by depositing 8, 10 and 12 layers were obtained by the refractive index measurement. It can be seen from the Table 5.1 that thickness of the films increased with increasing the number of coating process.

Table 5.1 Refractive index and thickness of $PbTiO_3$ thin films.

Number of the film coating	**Film refractive index**	Film thickness (μm)
8	1,3204	**3,168**
10	1,3200	**5,662**
12	**1,3180**	**6,550**

The film thickness effect on the dielectric constant (ε′) and the dielectric loss (tan(δ)) of lead titanate films at a constant frequency are shown in Table 5.2. The dielectric constant increased with increasing film thickness, which can be related with capacitance equation ($K \propto 1/d$) which is previously mentioned in chapter 2.

Table 5.2 Dielectric constant (ε′) and dielectric loss (tan(δ)) of $PbTiO_3$ thin films with different thickness at a frequency of 1 Hz.

Film Thickness (μm)	**(ε′)**	Tan(δ)
3,168	≈ 0	10^5 - 10^6
5,662	≈ 0	10^3 - 10^4
6,550	3 - 2	10^2 - 10^3

Figure 5.10, 5.11 and 5.12 show the variation of dielectric constant (ε′) and dielectric loss (tan(δ)) against frequency of a 6,550 μm, 5,662 μm and 3,168 μm thick films, respectively. It can be observed that as the frequency increased, the dielectric constant decreased to a critical value after which it is nearly constant, while dielectric loss increased. We have good agreement with reference (Bao et al., 2002). Inasmuch as the thickness of film and surface defects such as micro-cracks, increases in accordance with number of dipping, dielectric properties of the thin films strongly affected with this issue which cause large number of short-circuited contacts and so decreasing dielectric response, as demonstrated in reference (Liu et al., 1999 & Pintilie et al., 2003). As demonstrated in microstructural observation, cracking was less extensive in thinner films while very thick films, which were produced using viscous solutions, tended to peel off the substrate completely owing to residual stress. In contrast, the films fabricated using diluted solutions with solvent, are extremely uniform, dense, crack-free and pinhole-free.

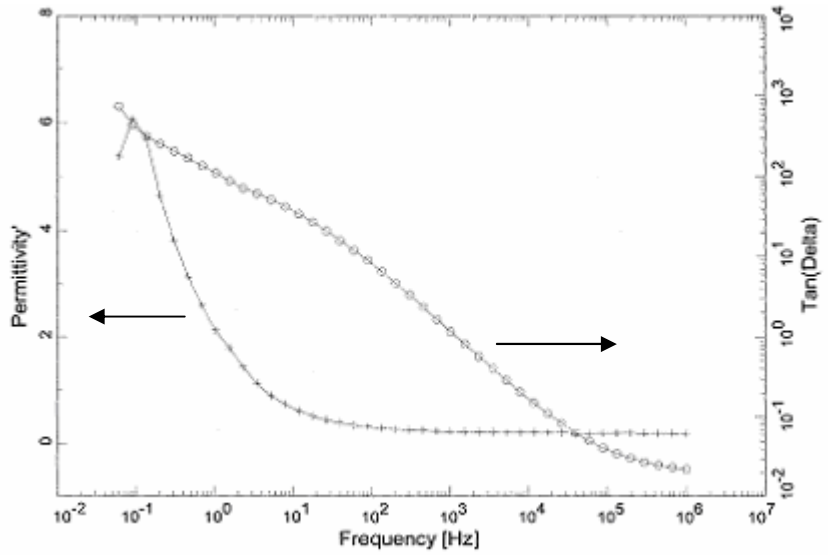

Figure 5.10 Variation of dielectric constant and loss with frequency for a 6,550 μm thick $PbTiO_3$ film annealed at 600 °C.

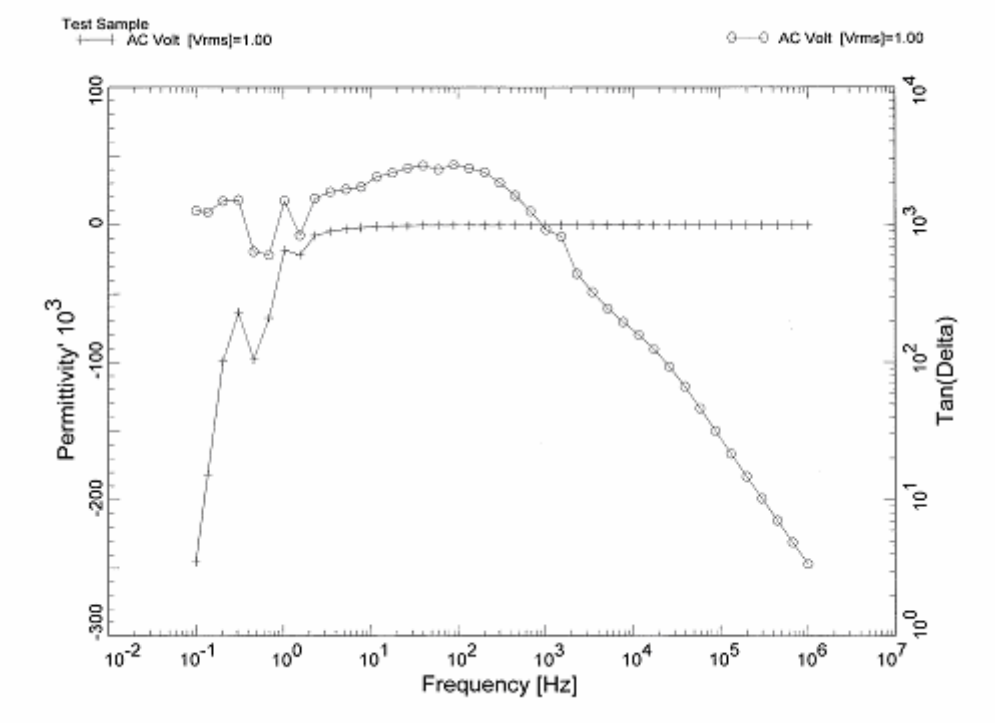

Figure 5.11 Variation of dielectric constant and loss with frequency for a 5,662 μm thick $PbTiO_3$ film annealed at 600 °C.

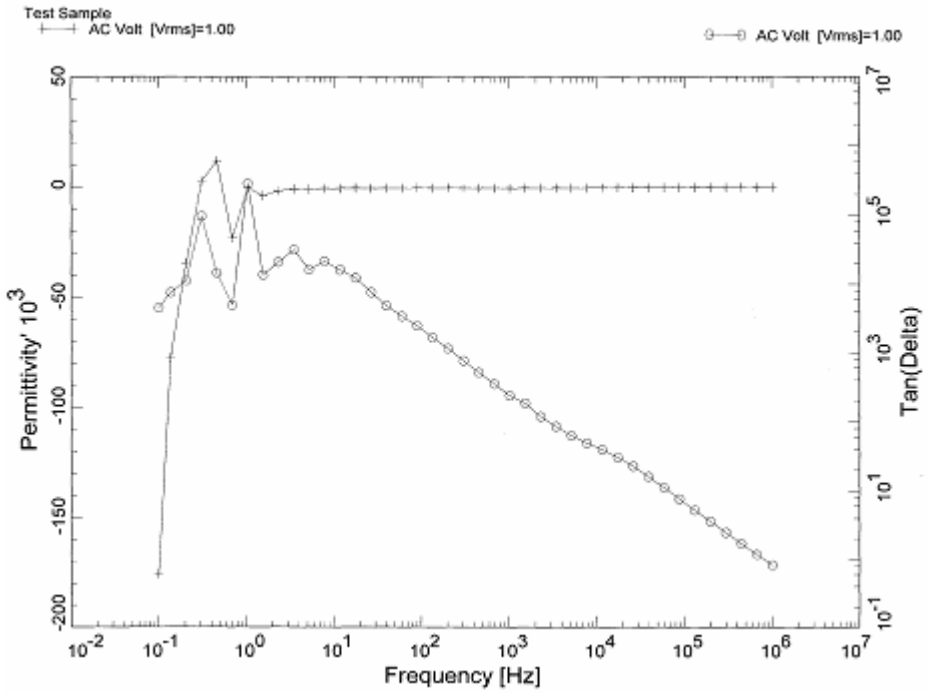

Figure 5.12 Variation of dielectric constant and loss with frequency for a 3,168 μm thick $PbTiO_3$ film annealed at 600 °C.

CHAPTER SIX
CONCLUSIONS

6.1. General Results

In this study, $PbTiO_3$ thin films were prepared on glass and stainless steel substrates by a sol-gel technique. The following conclusions are obtained from the experimental works:

1. The obtained solution becomes increasingly alkaline with increasing ethylene glycol. The pH value is an important factor that affects the formation of network structure during gelation.

2. Homogeneous lead titanate thin films were prepared by a sol-gel technique under simple production conditions.

3. The metastable intermediate oxides as indicated by the DTA curve and XRD patterns were formed about 400 °C. Perovskite phase started to develop at temperature ranging between 400 ~500 °C and the pure perovskite $PbTiO_3$ phase was fully developed at 600 °C for 1hr in air.

4. Morphology and microstructures of the thin films were found to be sensitive to the amount of solvent and film thickness. The optimum surface morphology of the film without any cracks or defects could be obtained in solution with maximum amount of solvent.

5. The value of dielectric constant (ε') and dielectric loss ($\tan\delta$) depended on film thickness. The film with highest thickness showed the highest ε' and lowest $\tan\delta$.

6.2. Future Plans

1. In order to obtain more homogeneous, crack-free, pinhole-free, and textured films, furnaces with controlled atmosphere should be used instead of air.

2. $PbLaZrTiO_x$ (PLZT) films can be produced instead of $PbTiO_3$ for same applications.

REFERENCES

Actuators, generators, sensors, transformers, & transducers, (n.d.). Retrieved March, 2005, from http://www.noliac.com/Standart_products.aspx.

Bao, D., Yao, X., Wakiya, N., Shinozaki, K., & Mizutani, N. (2002). Structural, dielectric, and ferroelectric properties of $PbTiO_3$ thin films by a simple sol-gel technique. *Materials Science and Engineering, B94*, 269-274.

Barsoum, M. W. (1997). *Fundamentals of ceramics.* New York: McGraw-Hill Companies, Inc.

Byun, C., Jang, J. W., & Lee, B. W. (1998). Correlation between the domain structure and ferroelectricity in $PbTiO_3$ thin films. *Materials Letters, 34,* 308-311.

Cheng, S. D., Kam, C. H., Zhou, Y., Que, W. X., Lam, Y. L., Chan, Y. C., et al. (2000). Sol-gel derived nanocrystalline thin films of $PbTiO_3$ on glass substrate. *Thin Solid Films, 375,* 109-113.

Dielectric, from wikipedia, the free encyclopedia, (n.d.). Retrieved March, 2005, from http://en.wikipedia.org/wiki/Dielectric.

Ferroelectricity & its applications, (n.d.). Retrieved October, 2004, from http://www.manep.ch/en/technological-challenges/ferroelectrics.html.

Fundamentals of piezoelectricity, (1996 – 2005). Retrieved October, 2004, from http://www.physikinstrumente.com/en/products/predetail.php.

He, X. Y., Ding, A. L., Zheng, X. S., Qiu, P. S., & Luo, W. G. (2003). Preparation of PZT (53/47) thick films deposited by a dip-coating process. *Microelectronic Engineering, 66*, 865-871.

Jordan, T. L., & Ounaies, Z. (September 2001). *Piezoelectric ceramics characterization.* Retrieved October, 2004, from http://www.techreports.larc.nasa.gov/icase-2001-28.pdf.

Kingery, W. D., Bowen, H. K., & Uhlmann, D.R. (1976). *Introduction to ceramic engineering* (2nd ed.). New York: John Wiley & Sons, Inc.

Lai, Y. C., Lin, J. C., & Lee, C. (1998). Nucleation and growth of highly oriented lead titanate thin films prepared by a sol-gel method. *Applied Surface Science, 125*, 51-57.

Liu, Y., Xu, C. N., & Watanabe, T. (1999). Preparation and characterization of preferred oriented PZT films on amorphous substrates. *Journal of Materials Science, 34*, 4129-4132.

Lu, C. J., Shen, H. M., & Wang, Y. N. (1998). Grain size effect on the phase transitions in oriented $PbTiO_3$ thin films deposited by the sol-gel method on (111) Pt/Si. *Materials Letters, 34*, 5-9.

Ma, W. H., Zhang, M. S., Shun, L., Chen, Y. F., & Ming, N. (1995). (001)-oriented $PbTiO_3$ ferroelectric thin films grown on Si by metal-organic chemical vapor deposition. *J. Phys.: Condens. Matter, 7,* 9075-9080.

Malic, B., Kosec, M., Smolej, K., & Stavber, S. (1999). Effect of precursor type on the microstructure of $PbTiO_3$ thin films. *Journal of the European Ceramic Society, 19,* 1345-1348.

Meng, X., Cheng, J., Ye, H., & Chu, J. (2000). Characterization of the crystallization behaviors in the $PbTiO_3$ thin films on Si substrates by an infrared spectroscopy technique. *Infrared Physics & Technology, 41*, 47-50.

Moulson, A. J., Herbert, J. M. (1990). *Electroceramics: Materials, Properties, Applications*. London: Chapman & Hall.

Phillips, J. R. (August 10, 2000). *Piezoelectric technology primer.* Retrieved January, 2005, from http://www.techonline.com/community/ed_resource/feature_article.

Pierre, A. C. (1998). *Introduction to sol-gel processing* (2nd ed.). Massachusetts: Kluwer Academic Publishers.

Piezoelectric ceramics properties & applications, (n.d.). Retrieved January, 2005, from http://www.morganelectroceramics.com/pzbook.html.

Piezoelectric impedance, (2005). Retrieved January, 2005, from http://www.efunda.com/materials/piezo/electronics/.

Piezo theory, (1998). Retrieved January, 2005, from http://americanpiezo.com/piezo_theory/index.html.

Pintilie, L., Boerasu, I., Gomes, M. J. M. 2003. Pereira, M. Properties of $Pb(Zr,Ti)O_3$ thin films deposited by sol-gel. *Thin Solid Films*, *xx, xxx-xxx.*

Prasad, E. S., Waechter, D. F., Blacow, R. G., King, H. W., & Yaman, Y. (2005). Application of piezoelectrics to smart structures. *II Eccomas Thematic Conference on Smart Structures and Materials.*

Reed, J. S. (1995). *Principles of ceramic engineering* (2nd ed.). New York: John Wiley & Sons, Inc.

Richerson, D. W. (1992). *Modern ceramic engineering* (2nd ed.). New York: Marcel Dekker, Inc.

Safari, A., Panda, R. K., & Janas, V. F. *Ferroelectric ceramics : processing, properties & applications,* (n.d.). Retrieved October, 2004, from http://www.rci.rutgers.edu/.

Schwartz, R. W. (1997). Chemical solution deposition of perovskite thin films. *Chem. Mater., 9* (11), 2325-2340.

Sparkler piezoceramics, (n.d.). Retrieved May, 2005, from www.sparklerceramics.com.

Tartaj, J., Moure, C., Lascano, L., & Duran, P. (2001). Sintering of dense ceramics bodies of pure lead titanate obtained by seeding-assisted chemical sol-gel. *Materials Research Bulletin, 36,* 2301-2310.

Wu, A., Vilarinho, P. M., Miranda Salvado, I. M., & Baptista, J. L. (1998). Seeding studies in PZT thin films. *Materials Research Bulletin, 33,* 59-68.

Yadav, H. O. (2004). Optical and electrical properties of sol-gel derived thin films of $PbTiO_3$. *Ceramics International, 30,* 1493-1498.

Zeng, X., Liu, Y., Wang, X., Yin, W., Wang, L., & Guo, H. (2002). Preparation of nanocrystalline $PbTiO_3$ by accelerated sol-gel process. *Materials Chemistry and Physics, 77*, 209-214.